Characterization of Spray-Drying Nozzles at Industrially Relevant Conditions

Continuation Proposal
2021

Primary Investigator: **Nasser Ashgriz**
PhD Students: **Isaac Jackiw & Siyu (Jerry) Chen**
Institution: **University of Toronto, Canada**

IFPRI
International Fine Particle Research Institute

UNIVERSITY OF TORONTO | Department of Mechanical and Industrial Engineering

Abstract

This proposal is a continuation of the presently IFPRI funded research, aimed at developing physically realistic models for atomization processes in swirl and twin-fluid nozzles with a focus on fluids with suspensions. The objectives of the present research are (i) spray characterization of liquids with solid suspension, and (ii) development of atomization models for fluids with suspensions. We will study suspensions with different particle types and sizes, solutions with significant elongational viscosity, surface tension, and molecular weight. We will use both pressure-swirl and twin-fluid nozzles in this study.

The second objective will be achieved by a set of basic studies on the breakup of ligaments either injecting a jet in a cross flow or by suspending a liquid bridge in a cross flow. The breakup dynamics will be recorded using a highspeed video. The cross-flow temperature will be changed to study the effect of heating on the breakup of the ligaments. Effects of fluid rheological properties as well as particle size and concentration in different suspension will be investigated.

Present Proposal

Background

The prior studies on the atomization of liquid with suspensions have identified the followings:

- Large particles in a slurry may separate from the droplets.
  - Glaser (1989) tested a slurry with particle sizes of 20 μm and concentrations up to 71 weight percent using prefilming-swirl nozzle. He found that the large solid particles separated from the water droplets.
  - Isenschmid (1992) compared the twin-fluid atomization of various suspensions with particle sizes of 4 to 16 μm and concentrations of 0 to 30 weight percent but did not show a clear influence of solid particles on the droplet size.
  - Mulham et al. (2001) found some separation of large solid particles from the liquid, but not for fine solid particles.
- Effect of particle size on the SMD is still not clear.
  - Yan et al. (2014) performed experiments on lime particle slurries using a pressure-swirl nozzle that showed that SMD increased with increasing solid percentages of lime slurry. Also, spray angle slowly decreased with increasing solid percentages of lime slurry. A twin peaks flux distribution was observed, which increased nonlinearly with increasing injection pressure.
  - Mulham et al. (2006) found a unimodeal size distribution for slurry suspensions with Dv_{50} >50 μm and a bimodal size distribution for Dv_{50} >50 μm.
    - For Dv_{50} < 50 μm, drop diameter was about the same as the pure carrier liquid droplet diameter. The effect of increasing carrier liquid viscosity on the atomization of suspensions with large and fine solid particles is similar to the observed effect on the atomization of pure suspension liquids, i.e., the drop diameter becomes larger with increasing the carrier liquid viscosity.

- For Dv_{50} >50 µm, one peak corresponded to the solid particle diameter in the suspension, and the other peak represented pure liquid spray size. At low injection pressures, the peak of the liquid droplet diameter was controlled by the solid particle size. Suspension with relatively fine solid particles showed a smaller diameter peak than the suspension with relatively large solid particles. At high injection pressures, this diameter peak was controlled by the gas velocity. In this region further break-up of liquid or suspension drops was similar to the fragmentation process of a pure carrier liquid.

- Generally, the shear thinning behaviour of the suspension viscosity, which increases with increasing solid concentration and decreasing solid particle size, makes the influence of the viscosity on the suspension break-up within a twin-fluid atomizer less important with increasing velocity of the atomizing gas (Glaser, 1989; Parthasarathy, 1999; Mulhem, 2004).

The following issues are raised based on the current data on the atomization of fluids with suspensions.

1- How does a solid particle separate from the solution? It is not clear whether the liquid is sheared off the solid particle or the particle separates during the breakup of the mixture. We will try to answer these questions by near nozzle closeup imaging.
2- Is there a correlation between the particle separation from the solution with respect to its size, the suspension concentration, and other solution rheological properties?
3- Does the SMD of the spray increases with an increase in solid particle size? There are conflicting results on this, as some show no increase, whereas some show an increase in SMD with particle size.
4- At what conditions does the unimodal size distribution turns into a bimodal size distribution? One study shows that this happens for Dv_{50} >50 µm. However, this value corresponds to their specific experiment. There is neither a criterion nor a correlation for a critical suspension parameter, at which point the size distribution becomes bimodal.
5- What are the differences between the suspension fluid atomization in pressure-swirl and twin-fluid atomization? In pressure-swirl atomization, a solution is converted into a thin sheet, which is then atomized into droplets, whereas in a twin-fluid atomization, a high gas velocity tears the solutions into droplets and ligaments. The influence of particles in each of these processes can be different. For instance, particles in a sheet may expedite preformation and breakup, whereas particles may not break off the core liquid in shearing process of twin-fluid atomization.

The present proposal is designed to address these questions.

Objectives

Objective 1. Spray Characterization of Liquids with Solid Suspension

There have been several requests from IFPRI members to perform tests with slurry fluids, as well as considering the effects of other rheological properties on the atomization. We propose to investigate the effect of the following specific properties on the atomization: **slurries with different particle types and sizes** to determine how the atomization is affected; **fluids having significant elongational viscosity**, which influences the breakup of the ligaments during the secondary atomization; **surface tension**, which was not specifically studied in the previous work; and **molecular weight**, which was also not studied in the previous work. We will use both pressure-swirl and twin-fluid nozzles in this study.

Objective 2. Development of Atomization Models for Fluids with Suspensions

Because of the complicated nature of the atomization process, it is still not possible to have a pure theoretical model for the atomization. Therefore, our goal is to develop semi-empirical models (physics-based models with experimentally determined constants) to predict the droplet sizes generated by the two types of nozzles that we have been testing: pressure-swirl and twin-fluid nozzles. We will develop correlations for both SMD and for the spray size distribution. The following tasks are planned to achieve this objective.

2.1. Correlations for Droplet Size Distribution

The PDF of the size distribution provides much more information than just the SMD. For example, an increase in viscosity may result in the formation a large number of large droplets, as well as a large number of small droplets, such that the SMD remains the same. The PDF is also used as an input into the CFD models for sprays. Our current study on high viscosity fluids has shown that the size distribution in such sprays can be bimodal. Therefore, a bimodal distribution function that accurately fits the data is needed. We will use the experimental data to develop correlations for the distribution functions for fluids with suspensions, in addition to the commonly presented correlations for the SMD.

2.2. Secondary Breakup of Ligaments of fluids with suspensions

The atomization process comprises of the breakup of a liquid into small ligaments. For high viscosity and polymeric fluids, the ligaments are long and may breakup again. This is referred to as the secondary atomization. In order to develop semi-empirical models for the atomization of liquids with suspension, we need to have experimental data on the breakup of ligaments of such fluids. In the proposed study we will perform basic study of the breakup of ligaments of fluids with suspensions, by suspending or jetting a ligament in a gaseous cross flow.

2.3. Perforation Based Model for Pressure-Swirl Nozzles

Based on studying the near nozzle images, we have developed a new atomization model for the pressure-swirl nozzles. The new model is based on a combination of a Kelvin-Helmholtz wave (KH) and a sheet perforation. In order to extend this model to fluids with suspensions, we need to determine the breakup length of the swirling sheet of such fluids, characterize the diameter of

the ligaments formed, and determine the number and frequency of the perforations on the sheet. These are planned for the proposed period.

2.4. Atomization in Twin-Fluid Nozzles

Two key advantages to the atomization models that we developed for twin-fluid nozzles in our previous project term are the ability to relate the rate of the deformation to the breakup and to predict the formation of ligaments in the spray. This allows for the opportunity to directly include rheological effects such as extensional viscosity in our models and to support their development by using what we learn in our experiments on the breakup dynamics of the ligaments and the spray characterization. Our previously developed model for the atomization of twin-fluid nozzles is comprised of the following processes: KH waves form on the jet that exits a nozzle and cause small droplets to break off its surface; the liquid core in the jet (the liquid left behind after KH droplets break off) goes through flapping instability, forming larger droplets with length scale of the flapping wavelength, and the secondary atomization process breaks the large droplets to smaller droplets. The breakup model is related to the rate of deformation of the waves. The advantages of modelling the spray in this way is the isolation of the slow wave growth from the fast wave breakup and the prediction of ligaments in the breakup, which previous models do not consider. While the development of the KH and flapping instabilities will be somewhat affected by the rheological fluids, the greater effect is expected to be on their breakup, especially when the extensional viscosity is high. Using what we learn in task 2.2 about the breakup dynamics of the ligaments, we aim to extend our existing models to include these effects.

Procedure

1. Spray Characterization of Liquids with Solid Suspension

The objective of this part of the research is the development of a more quantitative understanding of the influence of solid suspensions on atomization and droplet size distribution. The non-Newtonian rheological properties of the suspension play an important role in their disintegration process. We will measure the droplet size distribution for a range of suspension fluids. We plan to use Kaolin particles in our study. However, we will also use some of the suspension fluids of interest to IFPRI members (to be identified). The following part gives an example of the procedure on how we are going to generate the droplet size distribution.

We have been using Mavlern Spraytec Dropsizer to characterize our sprays. The Malvern instrument measures the volume percentage of droplets in different size ranges. Although volume percentage is valuable information, the droplet size distribution is a better indicator of the atomization process. The following is a brief discussion of the procedure we have used for obtaining the size distribution (more detailed information on the nozzles tested and conditions are provided in Appendix A).

Figure 1 shows histograms generated by Malvern Dropsizer for water and glycerin-water solutions at three different operating pressures. For almost all the testing cases, the histograms have one peak with a long tail on the left corresponding to the smaller droplets of less than 10 μm. The results show that as the injection pressure increases, the volume percentage of large droplets decreases and that of smaller droplets increases (e.g., the peaks move to the left).

Next, the volume percentage is converted to the volume distribution by dividing the height of each bin by the corresponding bin width. Figure 2 shows the volume distributions corresponding to the volume percentage of figure 1. The volume distribution amplifies the changes in the effect of droplet size on volume. Therefore, Fig. 2 shows bimodal distributions for the unimodal distribution of Fig. 1. The small tail in Fig. 1, results in the first peak in volume distribution curves. In order to find a size distributions corresponding to a volume distribution, we first guess a size distribution, and then calculate the volume distribution based on that and compare it with the experimental results. The parameters of the size distribution are then changed to match the experimental data. This procedure is simple for unimodal distributions, but more complex for bimodal distributions. We seek a mixture number distribution $f_0(d)$ that is the summation of two different unimodal distributions $f_{0,1}(d)$ and $f_{0,2}(d)$ as

$$f_0(d) = k_n f_{0,1}(d) + (1 - k_n) f_{0,2}(d),$$

such that their corresponding volume distributions have the following relationship

$$f_3(d) = k_v f_{3,1}(d) + (1 - k_v) f_{3,2}(d),$$

where k_n is the number ratio of the droplets generated by each distribution and k_v is the volume ratio of the droplets generated by each distribution. Since volume distribution based on a size distribution can be written as

$$f_3(d) = \frac{d^3 f_0(d)}{\int_0^\infty d^3 f_0(d) dd},$$

it can be shown that

$$k_n = \frac{k_v S_2}{S_1 + k_v (S_2 - S_1)},$$

where $S_a = \int_0^\infty d^3 f_{0,a}(d) dd\,, a = 1{,}2$. In order to fit the data, a distribution function is needed. We will use a lognormal distribution, which has the following form

$$f_0(d) = \frac{1}{d\sigma\sqrt{2\pi}} \exp\left(-\frac{1}{2}\left(\frac{ln(d/\mu)}{\sigma}\right)^2\right),$$

whose corresponding volume distribution is

$$f_3(d) = \frac{d^3}{e^{3\mu + 4.5\sigma^2}} f_0(d)$$

Figure 3 shows several results for fitting a mixture of lognormal distribution to experimental data. The mixture of lognormal distribution can not only follow the position of two peaks and the troughs properly for bimodal distribution (case 1 and case 5 as noted in the appendix A), but also fit to the unimodal distribution well (case 11). The mixture model has the form

$$f_3(d) = k_v f_{3,1}(d; \mu_1, \sigma_1) + (1 - k_v) f_{3,2}(d; \mu_2, \sigma_2)$$

with 5 parameters. For most of the cases, $k_v > 0.95$, which means the main peak is responsible for more than 95% fluid atomized. However, for most of the cases $k_n < 0.2$, which means that the small droplets take up more than 80% of the total number of droplets and the number distribution will be largely dominated by the small droplets.

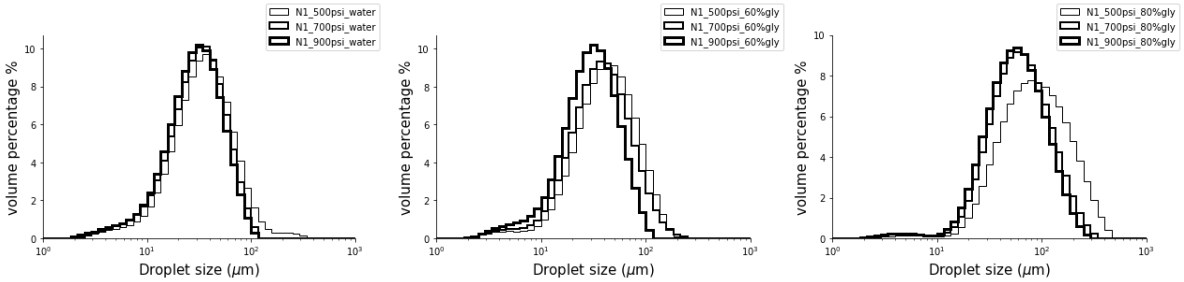

Figure 1: Volume percentage of each testing cases

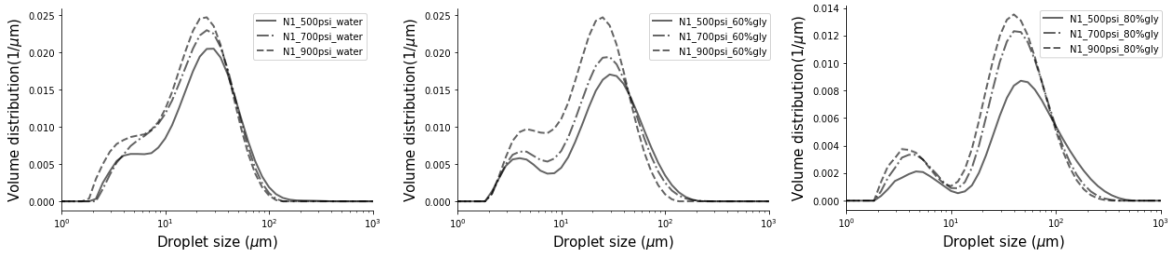

Figure 2: Volume distributions for all testing cases

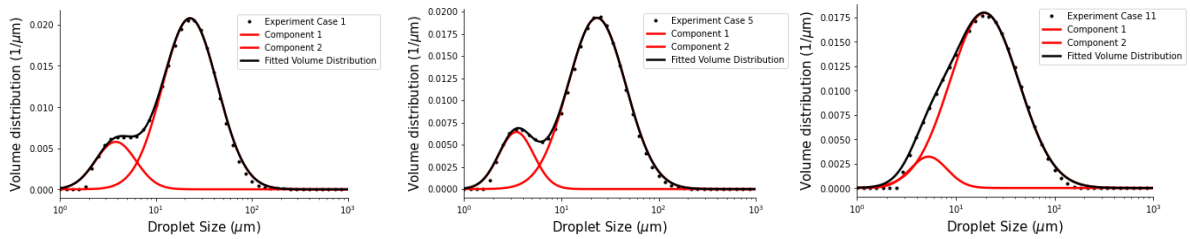

Figure 3. Fitting a mixture distribution of two lognormal distribution to experiment cases 1, 5 and 11, with nozzle diameters of 0.71mm, 0.71mm, and 1.07mm, and liquids of water, 60%gl-water, and water, respectively, and all at 700 psi injection pressure.

2. Development of Atomization Models for Fluids with Suspensions

2.1. Secondary Breakup of Droplets and Ligaments of Rheological Fluids

Our current near nozzle images of high viscosity liquid show the existence of long ligaments that may persist far downstream of the primary atomization region. This indicates a shortcoming in the traditional definitions of the atomization regions. Typically, the primary atomization results in the formation of droplets, while the secondary atomization is the breakup of those droplets. However, for viscous liquids, rather than only droplets being formed in the primary atomization region, ligaments are also produced that may undergo secondary breakup. Although the secondary breakup of droplets has been studied extensively in the literature, the secondary breakup of ligaments has not. Figure 4 shows an image downstream of the nozzle where large ligaments still exist.

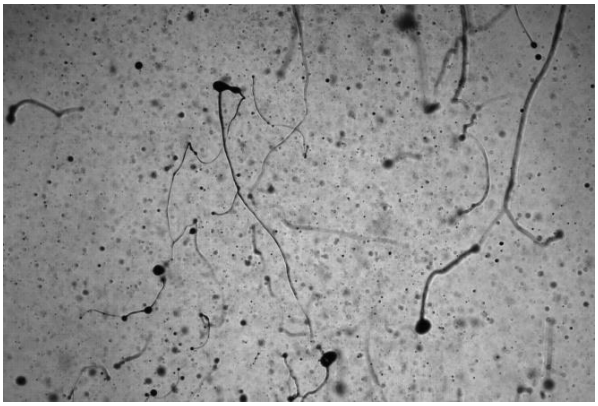

Figure 4: Image of a 0.5% CMC spray at 20-25mm downstream of the nozzle exit, showing the persistence of ligaments far downstream of the primary atomization region.

The question of the secondary breakup of the ligaments poses a few interesting problems, the most relevant of which is “do the ligaments break into small droplets or collapse into large droplets, and does this process occur over the timescales of spray drying?” If the timescale of the ligament secondary breakup is shorter than the drying process, then the resulting powder will have mainly spherical particles. However, if the ligaments do not break within the drying time, then the powder may have long, fibrous particles that decrease the quality of the powder. A better understanding of the secondary atomization of the ligaments will provide a basis for designing sprays to ensure that the ligaments do break within the drying time.

As we have found in our previous work, analyzing these ligaments based on commercial nozzle sprays is highly challenging. Due to the crowding of the images, ligament characterization and temporal tracking become difficult. Furthermore, there is no way to create controlled experiments of the ligament dynamics, as they are generated somewhat chaotically. By focusing on the fundamental aspect of the secondary breakup of single ligaments, we aim to provide models and understanding of the secondary breakup of ligaments that can be used as a basis for analyzing the complex ligament networks in commercial sprays more effectively.

We propose to study the fundamental behaviours of the secondary breakup of droplets and ligaments. The study of the breakup of droplets will be a direct continuation of our previous IFPRI term, which sought to understand and model the processes that lead to ligament formation and breakup. Some of the images that resulted from this study are shown in Fig. 5. The

secondary atomization model developed based on this study is already published Jackiw and Ashgriz (2021).

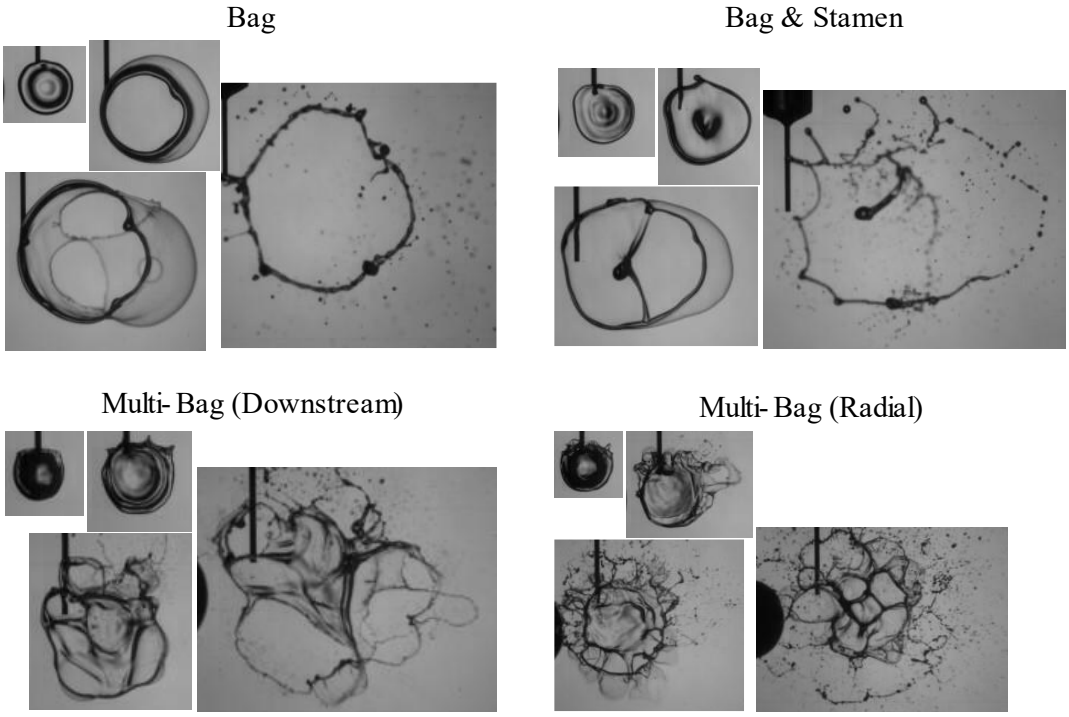

Figure 5: Images of droplet breakup for various morphologies showing the formation of ligaments.

To study the breakup of ligaments, we will generate small diameter ligaments of viscous, polymeric, and slurry fluids that we will expose to a variety of conditions such as a gaseous cross flow to study their breakup. Two methods that we can use to generate these ligaments are to study the breakup of a liquid jet in crossflow, which isolates the aerodynamic effects on the ligament breakup, or using the liquid bridge method, where we can add additional factors such as ligament stretching. These methods are illustrated in Figure 6. The dynamics of the ligaments will be captured using high-speed video so that the temporal behaviour of the ligaments can be resolved. Key factors to be determined in these experiments are the effects of the extensional viscosity on the breakup and the timescales of the ligament breakup in addition to the sizes generated. These factors are expected to be related by the critical conditions required for the ligament breakup or collapse, thus, we will aim to determine what the critical conditions are and what parameters affect or determine them.

In these experiments, we may also study the effects of elevated ambient temperatures. Since the primary atomization occurs rapidly for two-fluid nozzles, there is no significant heat transfer to the fluid during the primary atomization. However, since the ligaments in viscous sprays persist for a long time after they are formed, their dynamics may be affected by the elevated temperatures, either in the changing of the liquid properties due to heating or by the evaporation of the solvents in the liquid.

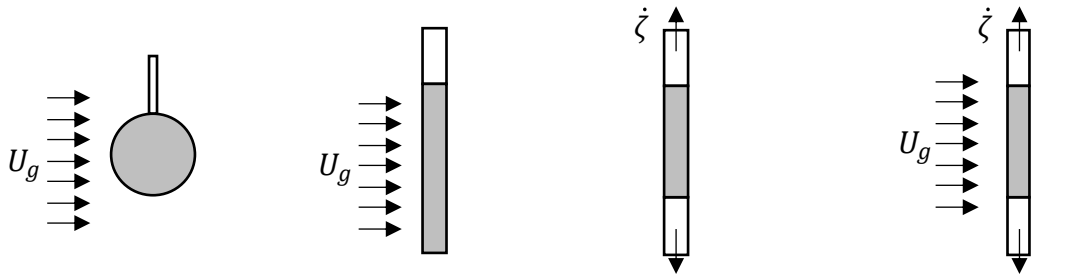

(a) Droplet in airflow (b) Jetted ligament in crossflow (c) Ligament bridge in extension (d) Ligament bridge in extension and airflow

Figure 6: Illustrations of experimental setups for study of droplet and ligament breakup

Similarly, the timescale for the primary breakup in pressure-swirl atomizer is short and there is no significant effect of heat transfer in this stage. A rough estimation can be made as the following. The velocity of liquid sheet for most cases studies is ~50 m/s. The primary breakup happens at around 15 mm downstream, therefore, the travel time is about 0.3ms. However, the heat transfer will influence the ligament breakup and the droplets generated. In addition, since the small diameter stream-wise ligaments usually form earlier and break up faster than the larger diameter span-wise ligaments in slurries and high viscosity cases, the effect of evaporation on the two types of ligaments is different. A rough estimation of the effect is given as the following. Consider an ambient temperature in the spray drying chamber of 100-200 °C. The spray size measurement is taken at 80 mm downstream, where the secondary breakup is almost completed. Therefore, the travel time from the primay breakup position to the the measurement point is about 1.3 ms. According to the D-square model for droplet evaporation, droplets less than 11.4 μm will fully evaporate at 80mm (using an evaporation constant of $\sim 0.1 \times 10^{-6} m^2/s$). Therefore, the droplets generated by streamwise ligaments may fully evaporate in the measurement position, whereas those generated by spanwise ligaments may not.

We have generated a large library of images of ligaments for sprays with different fluid properties and different nozzle operating conditions, such as ones shown in Fig. 7 for pressure-swirl nozzles. In these cases, there are two different length scales for the ligaments: larger diameter ligaments (red) in the spanwise direction, and small diameter ligaments (blue) in the streamwise direction. The large diameters are in the 100's microns, whereas, the small diameters are in 10's microns. Therefore, we will study breakup of ligaments in these size ranges.

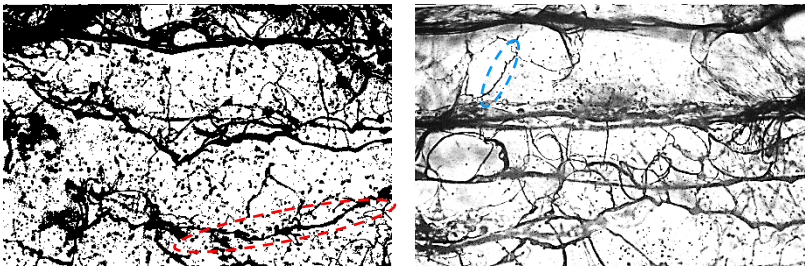

Figure 7. Large diameter spanwise ligaments (red) and small diameter streamwise ligaments (blue) in a pressure-swirl sprays.

2.2. Perforation Based Model for Pressure-Swirl Nozzles

Based on the near nozzle images, a new atomization model is proposed for the swirl nozzles. A perforation-based atomization model as depicted in Fig. 8 is proposed. The liquid sheet breaks up into droplets in the following steps:

1. As the high-speed swirling conical liquid sheet comes out of the orifice, surface wave is generated as it moves with respect to the ambient air due to the Kelvin-Helmholtz (KH) instability.
2. As the liquid sheet moves down stream, the amplitude of wave crests become larger, and these wave crests becomes the thick rims. Perforations appear on the liquid sheet surrounded by these thick rims.
3. As the conical sheet expands and the perforation grows, the conical sheet eventually forms a network of ligaments, with both stream-wise ligaments generated by the perforation and span-wise ligaments generated by thick rims.
4. When most of the stream-wise ligaments break into droplets, the liquid sheet disintegrates. The span-wise ligaments will last longer due to their larger diameters.

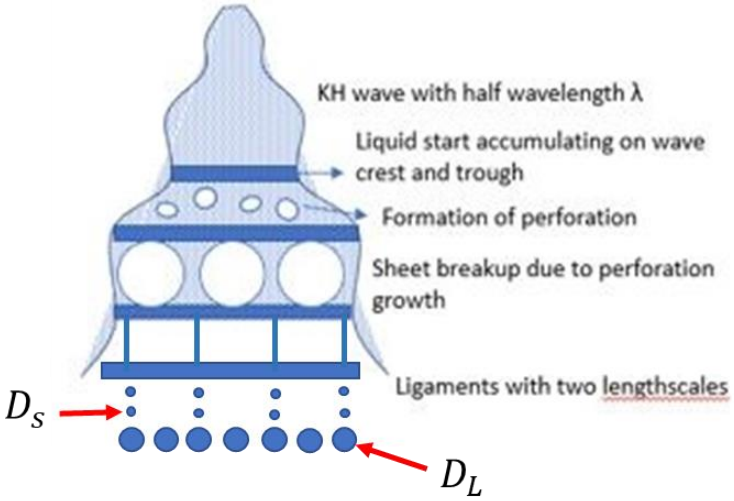

Figure 8. A schematic of the perforation-based atomization model

This breakup model provides two different length scales, which takes up different weight percentages: One based on the thickness of the thin sheet between the crests and troughs of the waves (D_S) with a total mass of m_S, and one based on the diameters of the crests and troughs (D_L) with a total mass of m_L and these can be given as

$$D_L = \sqrt{\frac{4m_c}{\pi^2 D_b}}, D_s = \sqrt{\frac{4(m - m_c)}{\pi n \lambda}}$$

where D_b is the breakup length, n is the number of perforations on the thin sheet and λ is the distance between the wave crests.

We will model the spray size distribution using two size distribution (PDF) each for one of the spray length scales. In order to complete this model, we need to determine correlations for the characteristic sizes of both the spanwise and the streamwise ligaments, in terms of the fluid

properties and the operating conditions. In order to develop a correlation that can be generalized to a wider range of fluids and operating conditions, the following tasks are planned

- Determine the frequency of perforations on the thin sheets with fluids with suspensions.
- Determine how much mass is accumulated at the wave crest
- Develop a theory for how long the sheet can stretch in Newtonian case
- Determine the breakup length of the fluids sheets with suspensions

Theses data will be combined with the ligament breakup model (Rayleigh-Plateau instability) for non-Newtonian fluids to generate a model for droplet size distribution. More detailed information on the testing cases and their results including droplet size distribution and near nozzle images are provided in Appendix A.

2.4. Atomization in Twin-Fluid Nozzle

Our currently developed model for the atomization of the twin-fluid nozzles comprises of the following processes:

- High-speed gas flow over the liquid breaks off small droplets from the surface of the liquid jet issuing from the nozzle based on Kelvin-Helmholtz (KH) instability. The droplet sizes are related to the wavelength of the fastest growing KH waves.
- The liquid core in the jet (the liquid left behind after KH droplet break offs) goes through flapping instability, forming larger droplets with length scale of the flapping wavelength.
- The secondary atomization process breaks the large droplets to smaller droplets. The following secondary atomization model is developed: The high-speed gas flow deforms the front of the droplet into a disk shape. The volume-fraction in the frontal disk determines the breakup morphology:
    - A model is developed that can predict the following morphologies: single bag and multibag breakup, as well as bag and stamen breakups. The breakup is related to the rate of deformation of the droplet.
    - Each disk shape droplet forms a bag with a relatively thick rim. The bag grows and eventually breaks forming small droplets, and the rim breaks forming larger droplets.
    - Rims are analogous to the ligaments seen in high-viscosity spray breakup.
- The final spray droplet size distribution is predicted based on the primary and the secondary atomization models.

The advantages of modelling the spray in this way is the isolation of the slow wave growth from the fast wave breakup and the prediction of ligaments in the breakup, which previous models do not consider. While the development of the KH and flapping instabilities will be somewhat affected by the rheological fluids, the greater effect is expected to be on their breakup, especially when the extensional viscosity is high. Using what we learn about the breakup dynamics of the ligaments, we aim to extend our existing models to include these effects. The data generated in objectives 1 and 2 will serve to validate and verify our models for the global spray breakup.

Further details on the developed twin-fluid nozzle is given in Appendix B.

References

Broumand, M., Shahzeb Khan, M., Yun, S., Hong, Z., Thomson, M.J., Development of an aqueous surrogate for the spray performance evaluation of viscous bioliquids, Experimental Thermal and Fluid Science 128 (2021) 110447.

Glaser, H. W., 1989 VDI Düsseldorf.

Isenschmid, T., 1992 Diss. ETH Nr. 9609.

Jackiw, I. M., and Ashgriz, N., "On Aerodynamic Droplet Breakup," J. Fluid Mech., **913**(A33), (2021).

Kim, H., Ko, T., Kim, S., Yoon, W., Spray characteristics of aluminized-gel fuels sprayed using pressure-swirl atomizer , Journal of Non-Newtonian Fluid Mechanics 249 (2017) 36–47.

Liu Z., and Reitz, R.D., "An analysis of the distortion and breakup mechanisms of high speed liquid drops," Int. J. Multiphas Flow 23, 631 (1997).

Mulhem, B. Fritsching, U. Schulte, G. and Bauckhage, "Characterisation of Twin-Fluid Atomisation for Suspensions," 2001 ILASS-2001 Zurich.

Mulhem, B., Schulte, G., Fritsching, U., Solid–liquid separation in suspension atomization, Chemical Engineering Science 61 (2006) 2582 – 2589.

Qian, L., Zhong, X., Zhu, C., Lin, J., An experimental investigation on the secondary breakup of carboxymethyl cellulose droplets, International Journal of Multiphase Flow 136 (2021) 103526

Ranger A.A., and Nicholls, J.A., "The aerodynamic shattering of liquid drops," AIAA J. 7, 285 (1969).

Schröder, J., Kraus, S., Rocha, B.B., Gaukel, V., Schuchmann, H.P., Characterization of gelatinized corn starch suspensions and resulting drop size distributions after effervescent atomization, Journal of Food Engineering 105 (2011) 656–662.

Theofanous, T.G., "Aerobreakup of Newtonian and viscoelastic liquids," Annu. Rev. Fluid Mech. 43, 661 (2011).

Yan, Y., Zhang, L., Pan, W., and Pu, G., Experimental Investigation of Atomizing Performance of Low Pressure Swirl Nozzle, Advances in Mechanical Engineering, Volume 2014, Article ID 782064, 10 pages.

Zhao, H., Liu, H-F, Xu, J-L, , "Secondary breakup of coal water slurry drops," Phys. Fluids, 23, 113101 (2011).

Zhao, H., Hou, Y-B., Liu, H-F., Tian, X-S., Xu, J-L., Li, W-F., Liu, Y., Wu, F-Y., Zhang, J., Lin, K-F., Influence of rheological properties on air-blast atomization of coal water Slurry, Journal of Non-Newtonian Fluid Mechanics 211 (2014) 1–15.

Appendix A - Pressure-Swirl Nozzle

A.1. Introduction

Most spray studies provide a mean size for the spray. One commonly presented mean size is the Sauter mean diameter, noted as SMD or d_{32}. The SMD is usually correlated with the operating conditions (injection pressure P, mass flow rate $\dot{m}$, etc.), fluid properties (liquid density ρ_l, viscosity μ, surface tension σ, etc.) and nozzle geometry parameters (orifice diameter d_{or}, etc.). For example, Tratnig and Brenn (2010) provided the following correlations for a swirl nozzle

$$\frac{d_{32}}{d_{SC}} = 3.074\left(\frac{\sqrt{P\rho_l}d_{SC}}{\mu}\right)^{-0.8505}\left(\frac{\mu}{\sqrt{\sigma d_{or}\rho_l}}\right)^{-0.7538}\left(\frac{h_{SC}}{d_{SC}}\right)^{-0.0574}\left(\frac{d_{or}}{d_{SC}}\right)^{-0.3496}\left(\frac{b_{SC}}{d_{SC}}\right)^{-0.0426}$$

where d_{SC} is the swirl chamber diameter, h_{SC} is the swirl chamber height and b_{SC} is the swirl chamber inlet width.

Wang and Lefebvre (1986) developed an empirical correlation with insight on the atomization process. They claimed that the atomization in a pressure swirl nozzle can be viewed as two stages. In the first stage, surface waves develop on the conical sheet due to instabilities. As the surface waves grow, they become large enough that some parts of the liquid break off from these surface waves and forms ligaments. The droplet size, SMD_1, generated at this stage is related to the Reynolds number, which indicates the strength of inertial force to breakup the sheet and Weber number, which governs the development of the surface wave. In the second stage, the rest of the sheet breaks up into ligaments as the surface wave grows when it moves downstream. The droplet size, SMD_2, generated at this stage is only related to the Weber number. The final SMD can then be predicted as a sum of these two $SMDs$. Fitting on their experimental data resulted in the following equation

$$SMD = SMD_1 + SMD_2 = 4.52\left(\frac{\sigma\mu^2}{\rho_g P^2}\right)^{0.25}(t_{or}cos\theta)^{0.25} + 0.39\left(\frac{\sigma\rho_l}{\rho_g P}\right)^{0.25}(t_{or}cos\theta)^{0.75}$$

where ρ_g is the density of the gaseous medium, t_{or} is the liquid sheet thickness at the exit of orifice, θ is the half spray cone angle. Xiao and Huang (2014) have noted that this correlation better fits their experimental data. Wang and Lefebvre's model is one of the earliest models indicating that there might be multiple breakup mechanisms in the atomization process of a pressure swirl nozzle.

Since the empirical correlation have limited insight on the actual atomization mechanism in the nozzle, they only make good prediction in a certain range of operating conditions and for the specific type of fluids used. A better understanding of the physical processes involved in these atomizers are needed to develop a model that is generalized enough to be applied to a wider range of operating conditions and fluids.

The current theoretical models describe the breakup of a liquid sheet in two steps: The breakup of liquid sheet into ligaments and the breakup of these ligaments into droplets. These models commonly use Kelvin-Helmholtz, Rayleigh-Plateau, and/or Rayleigh-Taylor instabilities as the cause of the liquid sheet breakup. The dominant wavelength λ_{max} (or wavenumber k_{max}) of the instability is then used to predict the size of the ligaments or droplets generated from the breakup. For example, Dombrowski and Johns (1963) developed the following relation for the diameter of the ligament, d_{lig}, formed by the breakup of a liquid sheet moving in the ambient gas with a velocity u:

$$d_{lig} = \sqrt{\frac{8a}{k_{max}}} = 2\left(\frac{4}{3f}\right)^{\frac{1}{3}}\left(\frac{C_t^2\sigma^2}{\rho_g\rho_l u^2}\right)^{\frac{1}{6}}\left(1 + 2.6\mu^3\sqrt{\frac{C_t\rho_g^4 u^8}{6f\rho_l^2\sigma^5}}\right)^{\frac{1}{5}}$$

where a is the half of the initial thickness of the liquid sheet, and the sheet is attenuating as $2a = C_t t^{-1}$, where C_t is a constant and t is the time. And f is a constant that appears from the surface wave of $y = A_0 e^f \sin(kx + \varphi)$, and it is assumed to be $f = 12$. The parameter f determines the place where the sheet breaks up and its value is set based on analogy to the jet breakup determined by Weber (1931). The ligaments then experience the Rayleigh-Plateau instability to breakup into the droplets. For a cylindrical ligament with a diameter of d_{lig}, the dominant wavenumber is given by

$$k_{max}d_{lig} = \frac{1}{2}\left(1 + \frac{3\mu}{\sqrt{\rho_l\sigma d_{lig}}}\right)^{-1/2} = \frac{1}{2}(1 + 3Oh)^{-1/2}$$

As the wave grows until its amplitude reaches the ligament radius, one droplet will be generated per wavelength. The SMD of these droplets is then given using a mass balance as

$$SMD = 1.882 d_{lig}(1 + 3Oh)^{\frac{1}{6}}$$

Another popular theoretical model developed for swirl nozzle is the linearized instability sheet atomization (LISA) model developed by Senecal et. al (1999). The main difference between LISA model and the model developed by Dombrowski and Johns (1963) is the way the dominant wavenumber k_{max} on the liquid sheet is determined. Instead of a 1-D force balance analysis, they performed a 2-D linear instability analysis. The maximum growth rate, ω_{max}, of the instability and its corresponding wavenumber, k_{max}, are found and used to evaluate the breakup time τ and breakup length L_b as: $\tau = \frac{1}{\omega_{max}}\ln\left(\frac{A}{A_0}\right)$, and $L_b = u\tau = \frac{u}{\omega_{max}}$, where A is the amplitude of the surface wave and A_0 is the initial amplitude of the surface wave. Similarly, $\ln\left(\frac{A}{A_0}\right) = 12$. Schmidt.et al (1999) applied this to a pressure swirl nozzle and found the sheet half-thickness t_b at L_b as

$$t_b = \frac{2t_{or}(d_{or} - t_{or})/cos\theta}{2L_b sin\theta + d_{or} - t_{or}}$$

According to the short wave assumption, one ligament is formed per wavelength. The diameter of these ligaments is found using a mass balance by

$$d_{lig} = \sqrt{\frac{16t_b}{k_{max}}}$$

These ligaments then break up into droplets with the same equation described above. Both of these models use a linearized instability analysis. Others, such as Clark and Dombrowski (1972), and Jazayeri and Li (2000), have developed higher order nonlinear instability models for the liquid sheet, which become too complicated to solve for the k_{max} directly, and therefore, they are hardly used for size prediction.

These atomization models usually overpredict the droplet size of the spray especially under high viscosity and high injecting pressure (Tratnig and Brenn, 2010). One reason that these models fail to make good prediction is that they oversimply the atomization mechanism. They assume that the liquid sheet stays intact until the instability waves grow enough to break the sheet. However, this is not the case in actual atomization processes. Experimental studies on liquid

sheet and swirl nozzle atomization show that perforations form on the liquid sheet. Perforations generate both stream-wise and span-wise ligaments in an liquid sheet with air-blast atomization (Stapper et.al in 1992). Sindayihebura and Dumouchel (2001) found perforations on the liquid sheet generated by a pressure-swirl nozzle using water solution of a non-Newtonian polymer. Loustalan et al. (2003) observed perforations in a spray of fuel atomizing at high injecting pressure. Therefore, new atomization models that better describe the mechanism of breakup are needed to improve droplet size prediction.
In this work, we present a set of experimental data on sprays generated by swirl nozzles, and a new model for the sheet atomization to better present the atomization process in these nozzles.

A.2. Experiment Setup

The experiments were carried out in the testing setup depicted in Fig. A1. A Hydra-Cell D10 pump was used to pump fluids from the tank at pressures up to 1000 psi. The pump was controlled by both a variable frequency controller (VFD) and a pressure regulating valve to adjust the pressure at the outlet. A high accuracy pressure gauge with ±1% accuracy was used to measure the inject pressure at the nozzle inlet. The fluid sprayed was collected below the setup for reuse. A curtain with an opening whose diameter allowed just the spray pass through without any blockage was mounted beneath the measuring region to prevent the equipment from measuring any recirculated droplets.

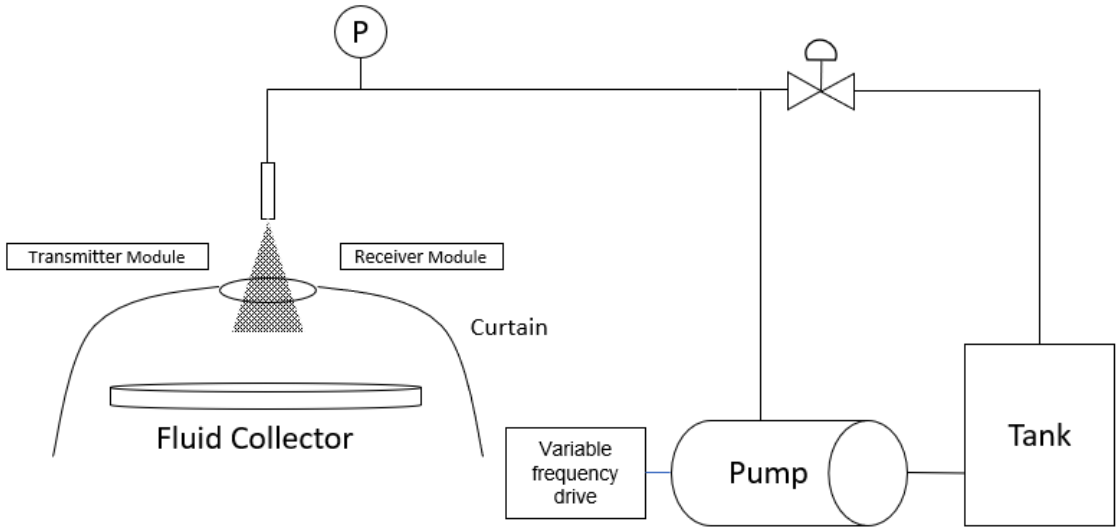

Figure A1: Schematic for Experiment Setup

The droplet sizes in the sprays were measured by the Malvern Spraytec Dropsizer, using a 300 mm lens. In this setup, the equipment could detect droplets from 0.1 μm to 900 μm. Malvern measures the volume distribution, which has to be converted to size distribution.

We used two different swirl nozzles with inserts, obtained from Spraying Systems. A smaller nozzle with an orifice diameter of 0.71 mm (N1), and a larger nozzle with an orifice diameter of 1.07 mm (N2). The testing fluids used were water, water-glycerin solutions and water-carboxymethyl cellulose (CMC) solutions with different concentrations. The surface tensions, viscosities and densities of water-glycerin solutions were obtained through a lookup table provided by Glycerin Producers' Association (1963) with linear interpolation at room

temperature (20 °C) as listed in Table A1. The properties of water-CMC solutions will be measured in the upcoming months. For each nozzle and each fluid, experiments were done at 3 different injection pressures of 500 psi, 700 psi, 900 psi. In order to measure the mass flow rate, the fluid was collected at the nozzle exit using a measuring cup for a certain time (more than 10 seconds) and weighted. This was repeated 3 times, and the average mass flow rate of the 3 runs was taken as the mass flow rate under the testing condition. Images are also taken at the nozzle exit to measure the spray angle. In total, eighteen different cases were tested. Measurements were taken at 8 cm downward from the nozzle exit. Each test case was repeated for at least 3 times to check the repeatability of the experiments. All the measurement result are listed in Table A2.

Table A1: Fluid properties of the testing fluids. The cells marked by * is to be measured in the future.

Fluid Type	Density (g/ml)	Viscosity (mPa.s)	Surface Tension (mN/m)
Water	0.997	1.005	71.68
60% glycerin/water	1.154	10.8	67.76
80% glycerin/water	1.209	60.1	65.49
0.25 % CMC/water	*	*	*
0.5 % CMC/water	*	*	*

Table A2: Measurement results for all testing cases. The cells marked by * are in progress.

Test Case	d_o (mm	Fluid Type	P (psi)	$\dot{m}$ (g/s)	Spray Angle	d_{32}(μm
1	0.71	Water	500	6.57	74.66	27.85
2	0.71	Water	700	7.70	78.72	22.75
3	0.71	Water	900	8.71	84.18	21.88
4	0.71	60% glycerin/water	500	9.90	54.68	29.68
5	0.71	60% glycerin/water	700	11.52	59.9	25.79
6	0.71	60% glycerin/water	900	13.02	61.92	22.28
7	0.71	80% glycerin/water	500	11.82	45.04	58.76
8	0.71	80% glycerin/water	700	13.02	49.95	45.44
9	0.71	80% glycerin/water	900	14.22	54.86	40.31
10	1.07	Water	500	18.74	73.02	30.97
11	1.07	Water	700	22.44	69.04	26.54
12	1.07	Water	900	24.94	70.14	24.18
13	1.07	60% glycerin/water	500	22.34	57.14	37.52
14	1.07	60% glycerin/water	700	26.39	61.58	32.83
15	1.07	60% glycerin/water	900	29.55	64.78	27.71
16	1.07	80% glycerin/water	500	24.50	53.19	50.18
17	1.07	80% glycerin/water	700	28.48	57.61	42.27
18	1.07	80% glycerin/water	900	31.94	62.11	37.38
19	0.71	0.25% CMC/water	500	*	*	77.71
20	0.71	0.25% CMC/water	700	*	*	53.71
21	0.71	0.25% CMC/water	900	*	*	42.92
22	0.71	0.5% CMC/water	500	*	*	174.0

23	0.71	0.5% CMC/water	700	*	*	109.2
24	0.71	0.5% CMC/water	900	*	*	83.33
25	1.07	0.25% CMC/water	500	*	*	55.66
26	1.07	0.25% CMC/water	700	*	*	45.47
27	1.07	0.5% CMC/water	500	*	*	76.45
28	1.07	0.5% CMC/water	700	*	*	61.08
29	1.07	0.5% CMC/water	880	*	*	54.14

A.3. Droplet Size Distributions

A.3.1 Raw Data from Malvern

The Mavlern Spraytec Dropsizer gives the droplet size measurement result in the form volume percentages of droplets in different bins, which are in the logarithmic scale. The histograms of all testing cases are shown on Fig. A2. For almost all the testing cases, the histograms have one peak with long tail on the left corresponding to the smaller droplets less than 10 μm. Increasing the orifice size will result in an increase in the span of the peak and a decrease in the maximum percentage of the peak. This indicates that the droplets generated have a wider range of sizes. For example, most peaks for the nozzle N1 are around 10%, while those for nozzle N2, which have a larger orifice diameter are around 8%. Atomizing high viscosity fluid with small orifice at low pressure have a similar effect, which is shown for the case of atomizing 80% glycerin/water solution with N1 nozzle at 500 psi. Furthermore, atomizing high viscosity polymeric fluid, such as 0.5% CMC solution, can result in a bimodal volume percentage histograms such as for N1 at all tested pressures and N2 at 500 psi. This indicates that the inertia force is not enough to counter the viscous force to break up the liquid properly into droplets. Increasing injection pressure can result in a change from bimodal volume percentage to unimodal volume percentage, for example for atomizing 0.5% CMC solution with N2 at 700 psi and 900 psi. The volume percentage of large droplets decreases and that of smaller droplets increases as the injection pressure increases. This is shown as the peak shifting to the left.

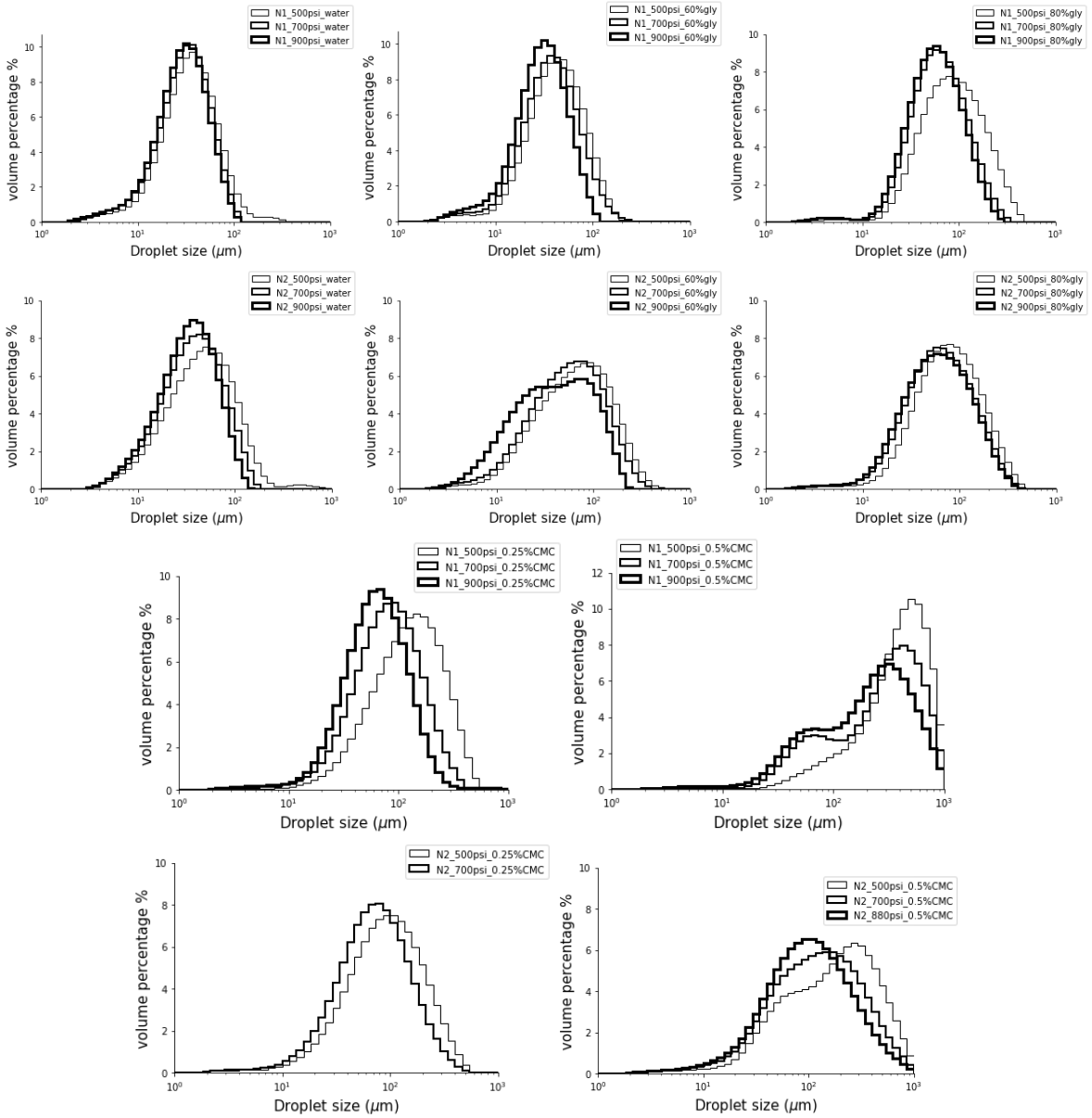

Figure A2: Volume percentage of each testing cases

A.3.2 Volume Distribution of Droplets

In order to get the volume distribution, the height of each bin is divided by the corresponding bin width and the results are shown in Fig. A3. As observed in Fig. A3, a unimodal volume histogram can become a bimodal volume distribution and a bimodal volume histogram can have three modes. It should be noted that the bin widths in the measurement result set by the Mavlern Spraytec Dropsizer are not equal. The bin width increases as the droplet size increases.

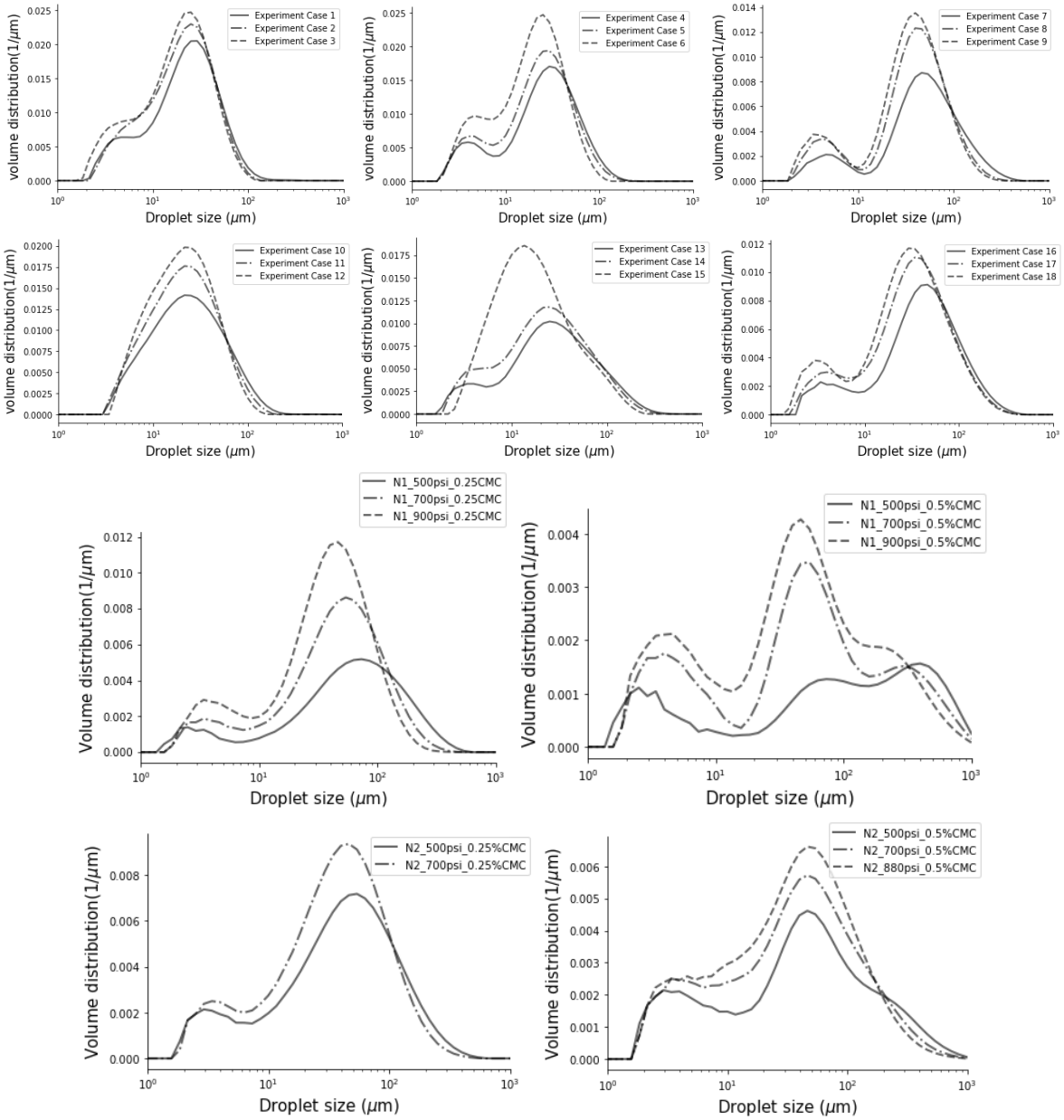

Figure A3. Volume distributions for all experiment cases

A.3.3 Cumulative Volume Distribution

The effect of operating conditions on the droplet size distributions is also presented in cumulative volume distribution in Fig. A4. The three horizontal dotted lines indicates the 90%, 50% and 10% of the total volume from top to bottom respectively. The x-coordinates of the intersections between these dotted lines and the accumulative volume distribution curve are the D_{v90}, D_{v50} and D_{v10}. As shown on the upper-left and upper-right plot, as the pressure increases, D_{v90}, D_{v50} and D_{v10} all decreases. The D_{v90} decreases most significantly among the three. This indicates that the number of large droplets decreases and the diameters of droplets vary in a smaller range. Increasing the orifice diameter of the nozzle does not have much effect on the D_{v10}, but largely increases D_{v90}. Similar effects can be observed in the lower-left plot as a result of increasing viscosity.

The cumulative volume distribution curves for both nozzles atomizing 80% glycerin/water solution at 700 psi are shown in the lower-right plot in Fig. A4. The D_{v10} of the spray generated by N2 nozzle is smaller than its counterparts, while the D_{v90} is larger. This indicates that the spray generated by N2 nozzle has a wider range of droplet sizes and there are more smaller droplets in the spray, which result in a smaller SMD than the spray generated by N1 nozzle.

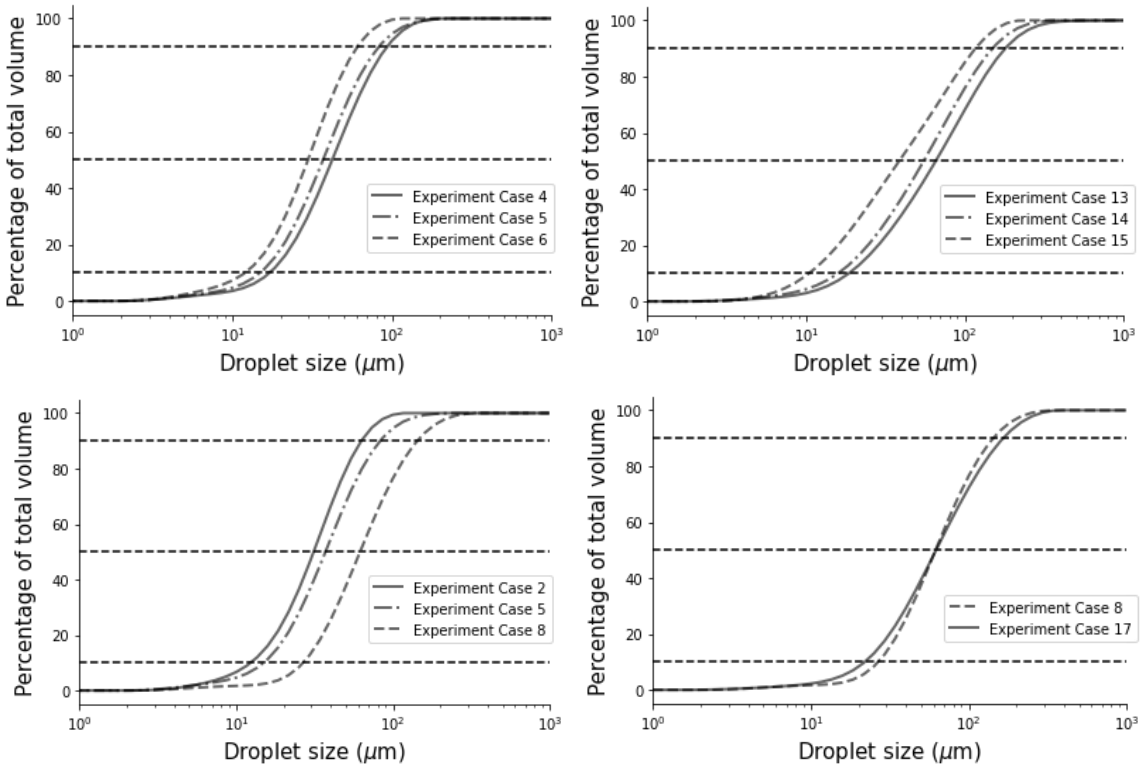

Figure A4. Comparison of accumulative volume distribution under different operating conditions

A3.4 Conversion of Volume Distribution to Size Distribution

In order to find the corresponding size distribution to a volume distribution, we will start with guessing a size distribution, and then calculate the volume distribution based on that and compare with the experimental results. The parameters of the size distribution are then changed to match the experimental data. This is complicated since we have a bimodal volume distribution.

We will seek a mixture number distribution $f_0(d)$ that is the summation of two different unimodal distributions $f_{0,1}(d)$ and $f_{0,2}(d)$ as

$$f_0(d) = k_n f_{0,1}(d) + (1 - k_n) f_{0,2}(d),$$

such that their corresponding volume distributions have the following relationship

$$f_3(d) = k_v f_{3,1}(d) + (1 - k_v) f_{3,2}(d),$$

where k_n is the number ratio of the droplets generated by each distribution and k_v is the volume ratio of the droplets. Since volume distribution based on a size distribution can be written as

$$f_3(d) = \frac{d^3 f_0(d)}{\int_0^\infty d^3 f_0(d) dd},$$

it can be shown that

$$k_n = \frac{k_v S_2}{S_1 + k_v(S_2 - S_1)}$$

where $S_a = \int_0^\infty d^3 f_{0,a}(d)dd\,, a = 1{,}2.$

As a result, as long as a bimodal distribution is fit to the volume distribution, their corresponding number distribution can be calculated. Although there are some methods developed for fitting a mixture model to the bimodal distribution, the author found that the performance of many of them largely rely on the initial value picked for these methods and it needs lots of effort to find the best initial guess to fit the bimodal distribution properly. Since the goal is to determine the parameters in the mixture model to fit the bimodal distribution properly rather than develop an algorithm with good mathematical base, the following method is used by the author. The main idea is to fit a distribution to the main peak first, and then adjust the ratio between two distributions to fit the residual, For a bimodal volume distribution function $f_3(d)$, we first guess the ratio k_v, then fit the main peak (the peak for larger droplets) by approximating the mean and variance for the main peak These values are used as an initial guess, and the parameters are optimized by minimizing the distance between the main peak and fitted distribution $f_1(d)$. The distance used in this work is the Earth Mover Distance (EMD) as:

$$EMD_1 = \int_{d_t}^{\infty} \left| f_3(d) - k_v f_{3,1}(d) \right| dd$$

where d_t is the diameter corresponding to the local minimum value in the bimodal distribution at the trough of volume distribution to separate the main peak and minor peak. Then the residual of the distribution is found: $r(d) = f_3(d) - k_v f_{3,1}(d)$, and parameters in $f_{3,2}(d)$ are optimized with similar method:

$$EMD_2 = \int_0^{\infty} \left| r(d) - (1-k) f_{3,2}(d) \right| dd$$

The above process is then repeated to minimize the total distance between the bimodal distribution and the mixture model, which optimizes the ratio k.

In order to fit the data, a distribution function is needed. One of the popular number distributions used in the literature is the Gamma distribution with 2 parameters α and β:

$$f_0(d;\alpha,\beta) = \frac{\beta^\alpha}{\Gamma(\alpha)} d^{\alpha-1} e^{-\beta d}$$

For example, Villermaux et. al. (2004) found that the number distribution of droplets generated from a ligament with size d_{lig} is a gamma distribution with 2 parameters as

$$f_0\left(d;\kappa,\nu,d_{lig}\right) = \frac{1}{\kappa d_{lig}} \frac{\nu^\nu}{\Gamma(\nu)} \left(\frac{d}{\kappa d_{lig}}\right)^{\nu-1} \exp\left(-\nu \frac{d}{\kappa d_{lig}}\right)$$

where κ and ν are determined empirically from experiment, in which the corresponding functions are $\alpha = \nu, \beta = \nu/\kappa d_{lig}$. The corresponding volume distribution based on the original size distribution parameters can be written as

$$f_3(d;\alpha,\beta) = \frac{\beta^{\alpha+3} d^{\alpha+2} e^{-\beta d}}{\Gamma(\alpha+3)} = \frac{\beta^{\alpha'}}{\Gamma(\alpha')} d^{\alpha'-1} e^{-\beta d},$$

which is also a Gamma function with $\alpha' = \alpha + 3$. However, as it shown on Fig. 10, a mixture distribution with two Gamma distribution does not fit well to experiment case 5. When fitting one Gamma component to the peak for larger droplets, although it fits the peak on right-hand side properly, its value is greater than the experimental data on the left-hand side, which makes it

impossible to find a mixture distribution by adding another Gamma component whose value is always positive. Another issue is, an α' value less than 3 will result in a negative α value when converting the volume distribution back to number distribution, which is unrealistic. Although Yongyingsakthavorn et. al (2008) successfully fit a mixture distribution with generalized Gamma distributions for an ultrasonic nozzle with smaller flow rate, a mixture distribution of Gamma distributions does not fit for the swirl nozzle at operating conditions tested in this work as shown in Fig. A5.

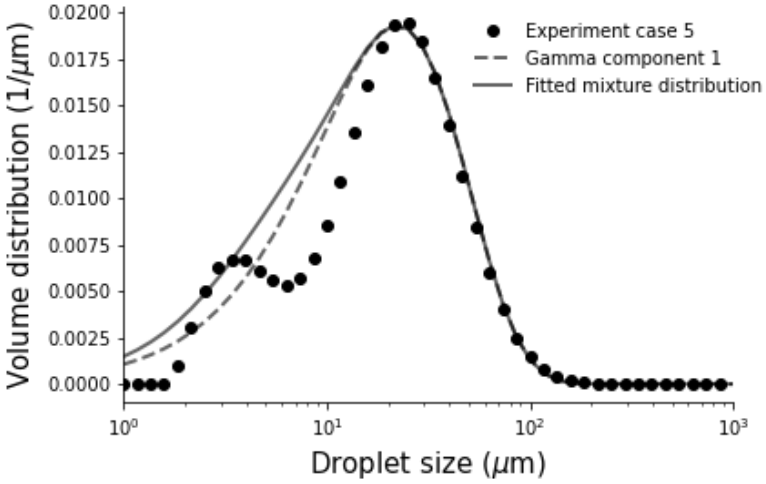

Figure A5. Fitting a mixture distribution of two Gamma distribution to experiment case 5. One of the components has a greater value than the experimental distribution in certain range.

Since Gamma distribution did not work well, we tried the lognormal distribution, which has the following form

$$f_0(d) = \frac{1}{d\sigma\sqrt{2\pi}} \exp\left(-\frac{1}{2}\left(\frac{ln(d/\mu)}{\sigma}\right)^2\right)$$

whose corresponding volume distribution is

$$f_3(d) = \frac{d^3}{e^{3\mu+4.5\sigma^2}} f_0(d)$$

Figure A6 shows several results for fitting a mixture of lognormal distribution to experimental data. The mixture of lognormal distribution can not only follow the position of two peaks and the troughs properly for bimodal distribution (case 1 and case 5), but also fit to the unimodal distribution well (case 11). The mixture model has the form

$$f_3(d) = k_v f_{3,1}(d; \mu_1, \sigma_1) + (1 - k_v) f_{3,2}(d; \mu_2, \sigma_2)$$

with 5 parameters. The parameters fitted for each case and the corresponding k_n are listed in Table A3.

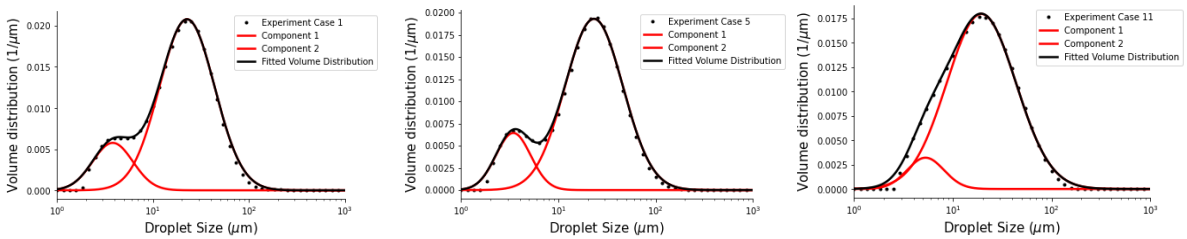

Figure A6. Fitting a mixture distribution of two lognormal distribution to experiment case 1, case 5 and case 11.

Table A3: Parameters in fitted mixture distribution of lognormal distributions

Case	k_v	k_n	σ_1	μ_1	σ_2	μ_2	d_{32} (μm)	Experimental Result (μm)
1	0.97	0.173	0.66	9.5	0.483	2.4	24.19	27.85
2	0.96	0.234	0.636	9.3	0.468	2.869	21.92	22.75
3	0.955	0.132	0.636	8.8	0.547	1.987	19.92	21.88
4	0.98	0.138	0.685	10.4	0.383	2.5	28.82	29.68
5	0.975	0.166	0.685	9.1	0.413	2.45	25.12	25.79
6	0.955	0.152	0.612	9.9	0.453	2.6	20.76	22.28
7	0.99	0.088	0.734	16.2	0.433	2.72	54.97	58.76
8	0.985	0.066	0.636	17.6	0.438	2.48	41.49	45.44
9	0.985	0.073	0.66	14.8	0.432	2.28	37.70	40.31
10	0.985	0.749	0.88	4.5	0.433	3.873	29.41	30.97
11	0.98	0.666	0.807	5.3	0.428	3.677	25.17	26.54
12	0.965	0.594	0.734	6.7	0.383	4.534	23.36	24.18
13	0.994	0.425	0.977	3.7	0.333	2.16	37.30	37.52
14	0.99	0.471	0.977	3.2	0.373	2.26	31.67	32.83
15	*	*	*	*	*	*	*	27.71
16	0.99	0.075	0.782	12	0.498	1.938	48.40	50.18
17	0.986	0.102	0.807	8.8	0.542	1.766	38.76	42.27
18	0.989	0.133	0.831	7.3	0.408	1.913	35.85	37.38

For most of the cases, $k_v > 0.95$, which means the distribution which has a larger μ is responsible for more than 95% fluid atomized. However, for most of the cases $k_n < 0.2$, which means that the small droplets take up more than 80% of the total number of droplets and the number distribution will be largely dominated by the small droplets. As a result, the corresponding number distributions may appear unimodal for a bimodal volume distribution. This can also explain why a single unimodal distribution cannot fit the number distribution of droplets in swirl nozzle properly (Tratnig and Brenn, 2010).

One reason for the huge number of small droplets is the uneven bin sizes in the result from the Dropsizer. Since the bins are in logarithmic scale, the bin width increases as the droplet size increases. Figure A7 shows the volume distribution converted from a volume distribution plot with the same height for all bins. It shows that the same percentage for smaller particles (those below 10 μm) resulted in a much larger value in volume distribution than that for larger particles. This indicates that the number of smaller particles, especially those less than 10 μm, is extremely prone to small errors.

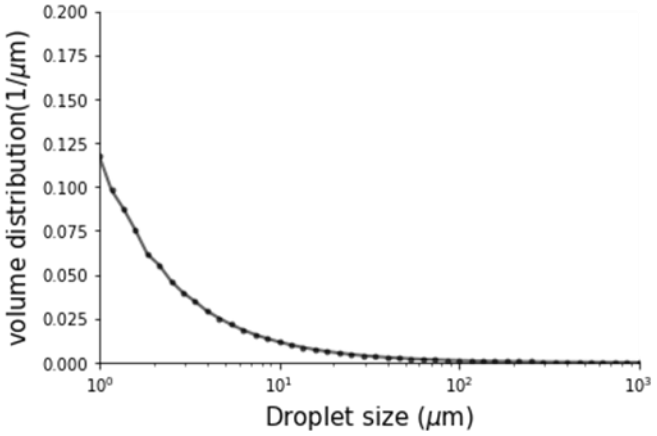

Figure A7. Volume distribution converted from a volume distribution plot with same height for all bins

A.4. Characteristic Droplet Sizes

The SMD of all the testing cases are plotted versus injecting pressure in Fig. A8, which shows that the SMD decreases as the injection pressure increases. The N1 nozzle, which has a smaller orifice diameter, generates finer droplets than the N2 nozzle for low viscosity fluids, such as water and 60% glycerin/water solution. However, when atomizing high viscosity fluids, such as 80% glycerin, N1 generates much larger droplets than N2.

The empirical correlation usually has the form of the power law. A dimensional analysis is carried out to study the relationship between the SMD and relevant parameters in the experiments for water and water-glycerin solutions. In order to calculate the non-dimensional groups such as Re and We, the velocity of the liquid sheet needs to be determined. Consider a fluid enters a pressure-swirl nozzle with a swirl insert at an injection pressure P. The liquid forms a swirling conical liquid sheet at the nozzle exit.

For a swirl nozzle, the mass flow rate of is written as $\dot{m} = (\rho U \cos\theta)\, \pi t_{or}(d_o - t_{or})$ where U is the total velocity of the sheet. However, since the size of the air core is hard to measure directly, the sheet thickness remains unknown, which makes it hard to calculate velocity U directly from the mass flow rate. The sheet velocity is determined using the pressure at the nozzle inlet P as $U = k\sqrt{2P/\rho}$, where k is the discharge coefficient. Although there are numerous methods to calculate the discharge coefficient in literature, they are all empirical and different from each other. As a result, the Re and We are modified to be as Re_p and We_p based on the inlet pressure, which is directly measured from the experiment. Since $P \sim \rho u^2$, $Re_p = \sqrt{P\rho}d_0/\mu$, $We_\rho = Pd_0/\sigma$. The correlation found for the non-dimensional SMD is

$$\frac{d_{32}}{d_o} = 42.52 Re_p^{-0.151} We_p^{-0.519} \tag{4}$$

The comparison between the experimental result and predicted SMD is shown in Fig. A9 on the left. The R^2 score for the correlation is 0.853, indicating a good result. However, the plot shows that there are 3 datapoints off the trends from the rest of the points. These datapoints are the experiments for the N1 nozzle, which has a small orifice diameter, atomizing 80% glycerin/water solution. If these datapoints are excluded, the new correlation found is

$$\frac{d_{32}}{d_o} = 7.37 Re_p^{-0.103} We_p^{-0.404} \quad (5)$$

The R^2 score improves to 0.894. This indicates that atomizing highly viscous fluid using nozzles with small orifice size may result in a different atomizing behaviour, generating larger droplets.

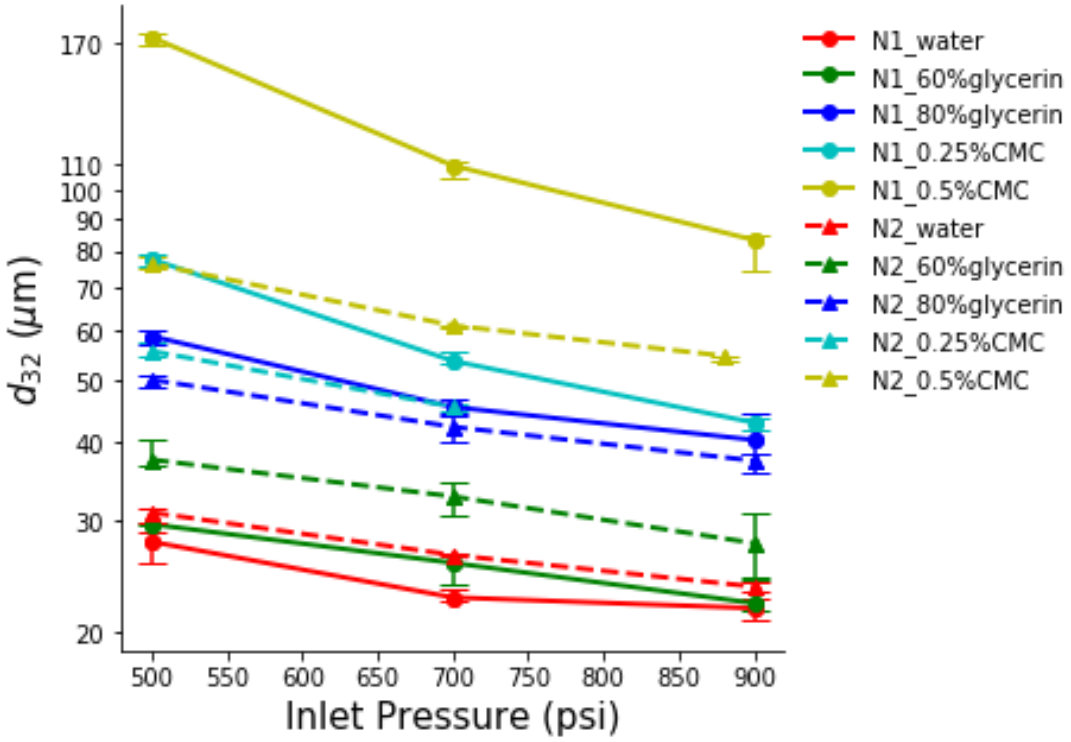

Figure A8. SMD versus Injection pressure for all testing cases.

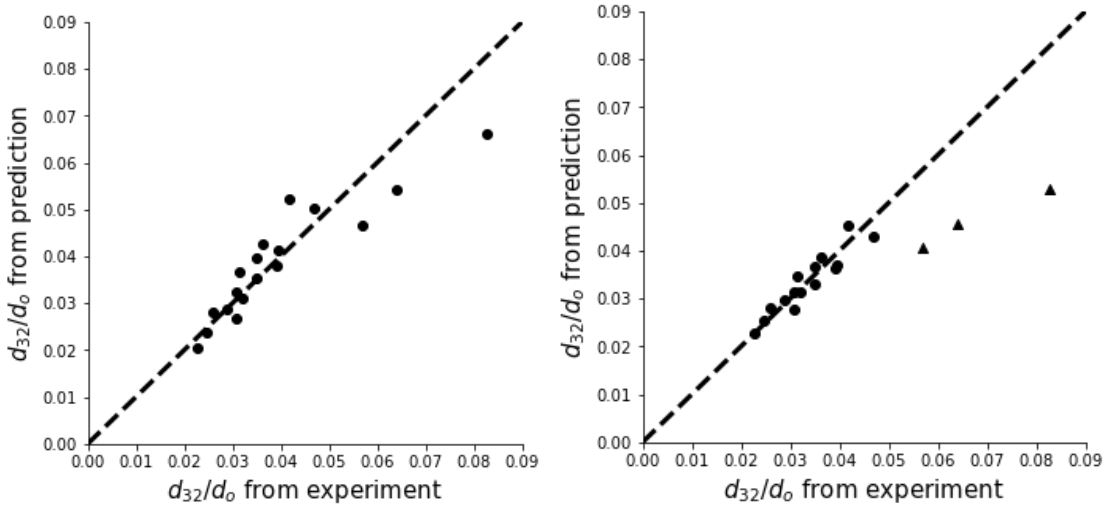

Figure A9. Comparison of non-dimensional SMD between experiment and prediction. Left: Correlation fit with all the data. R^2 = 0.853. Right: Correlation fit with data excluding ones from N1 nozzle, 80% glycerin (triangle points) R^2 = 0.894.

The comparison between the d_{32} calculated from LISA model and the d_{32} measured from the experiments for the current work is shown in Fig. A10. LISA model tends to overpredict the droplet diameters in most cases, which is also true for Tratnig and Brenn's data (2010). One main reason, also pointed out by Tratnig and Brenn (2010), LISA model overpredicts the breakup length in these cases. The breakup length predicted by LISA model for high viscosity fluid is 60~80 mm, while the near nozzles images show that the liquid sheet is already broken up into a web of ligaments within 20 mm for all the testing cases. A comparison between the breakup length measured and that predicted by LISA model is listed in Table A4. Such difference comes from the assumption that the liquid sheet stays intact until its thickness is attenuated less than twice the amplitude of the surface wave. In addition, according to LISA model, a shorter breakup length will result in a larger sheet thickness at the breakup, and thus, larger droplets. However, the experiments shows that not only the breakup length is smaller than predicted, but the d_{32} is smaller than that predicted by LISA model. As a result, it is important to study the breakup mechanism and see how it differs from what depicted by the LISA model.

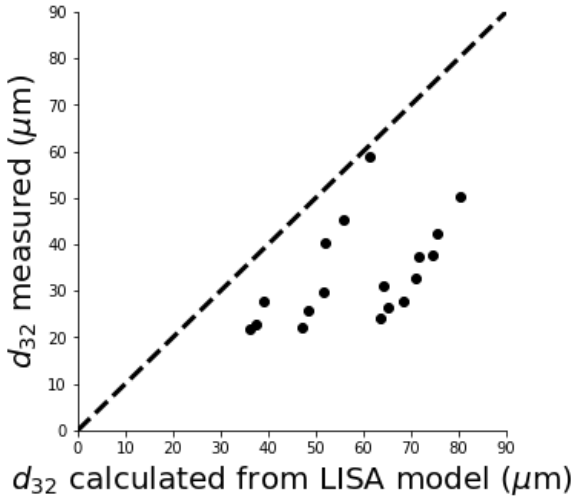

Figure A10. Comparison between d_{32} calculated from LISA model and experiment.

Table A4: Comparison of breakup length between experiment measurement and LISA model prediction.

Test Case	Breakup length predicted by LISA model (mm)	Breakup length measured (mm)	$d_{32}(\mu m)$
1	20.35	6.13	27.85
2	14.59	5.95	22.75
3	11.27	5.49	21.88
4	32.12	7.6	29.68
5	24.30	7.23	25.79
6	19.80	6.51	22.28
7	77.52	16.79	58.76
8	63.39	14.20	45.44
9	54.26	13.11	40.31
10	18.55	8.74	30.97

11	13.48	*	26.54
12	10.65	7.16	24.18
13	32.06	8.96	37.52
14	24.14	8.28	32.83
15	19.69	7.94	27.71
16	79.07	14.83	50.18
17	63.47	14.24	42.27
18	53.85	13.74	37.38

A.5. Atomization Mechanism in Pressure-Swirl Nozzle

Table A5 shows the images of the water spray atomizing with nozzle N1 at different pressures. The liquid sheet is not intact before the liquid sheet breaks up. The earliest observable perforation on the conical sheet is about 2 mm from the nozzle exit. These perforations occurred on the liquid sheet surrounded by the thicker rims, which is mostly span-wise. As a perforation grows, it will either be limited by the thick rims surrounding it or coalesce with its neighboring perforations and form stream-wise thick ligaments. As the sheet getting thinner and perforations growing, the liquid sheet will eventually become a web of ligaments. The stream-wise ligaments generated by the perforations usually have a smaller diameter compared to the rims and they tend to break faster in the atomization process. The sheet eventually breaks when most of the stream-wise ligaments break into droplets. The thick rims will then breakup into several shorter ligaments and then into droplets. Those shorter ligaments are still aligned in the span-wise direction as those rims.

Table A5: Near nozzle images for water spray atomizing with nozzle N1 at different pressures.

Z(Mm)	N1 - Water - 500PSI	N1 - Water - 700PSI	N1 - Water - 900PSI
0	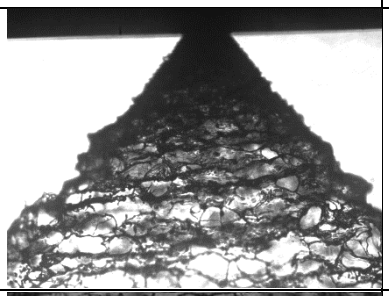	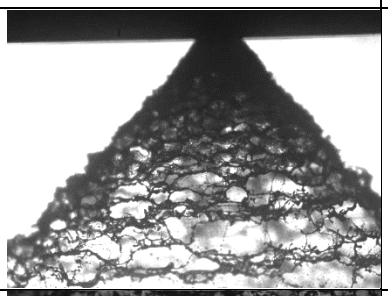	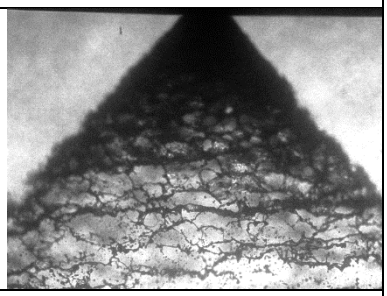
4.98	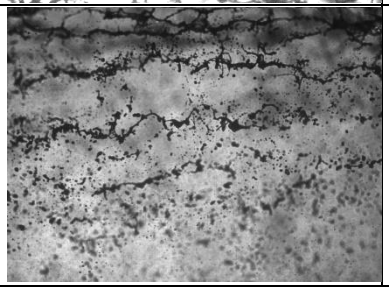	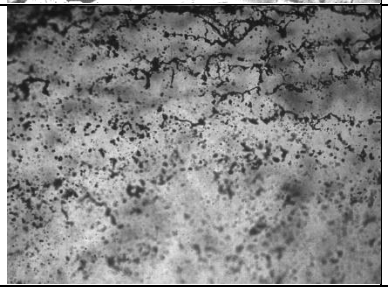	

Table A6 shows the images of spray with 60% glycerin/water solution for atomizing with nozzle N1 at different pressures. It can be observed from the edge of the cone that, the wavelength on the liquid sheet is larger compared to that of water spray. In addition, the amplitude at the wave crests is larger than that of water spray. It implies that the span-wise rims are thicker than that in the water spray, which is responsible for the larger droplet sizes. These thicker rims stay in the form of long ligaments while those stream-wise thin ligaments have already break up into multiple droplets.

Table A6: Near nozzle images for 60% glycerin/water spray atomizing with nozzle N1 at different pressures.

Z(mm)	N1 – 60% glycerin - 500PSI	N1 – 60% glycerin - 700PSI	N1 – 60% glycerin - 900PSI
0	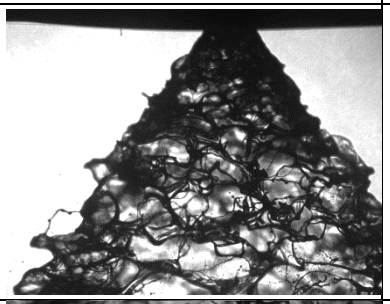	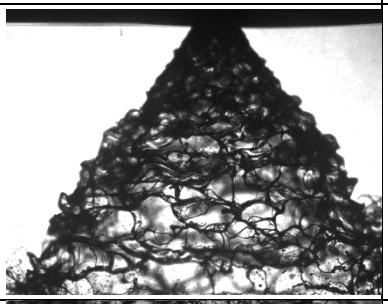	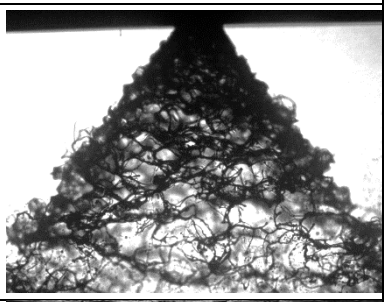
4.98	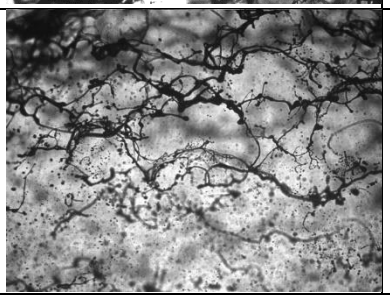	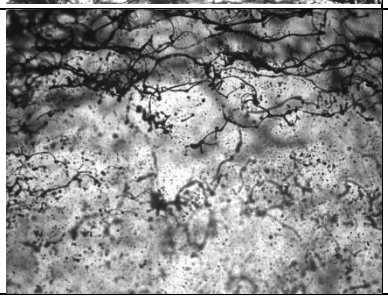	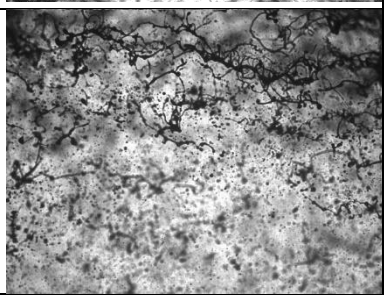

Table A7 shows the images of spray with 80% glycerin/water solution for atomizing with nozzle N1 at different pressures. The edge of the cone at the nozzle exit is smooth due to the high viscosity of the fluid. At 4.98 mm downstream, the amplitude of the wave crests starts to increase and the wave crests becomes thicker. In addition, the distance between the two consecutive wave crests increases. Take the spray atomizing at 700 psi as an example. It can be measure in the frame at 9.96 mm downstream that the distance between two wave crests is about 2 mm, which is much larger than the Kelvin-Helmholtz wavelength (481 μm). Compared to the lower viscosity cases, the thicker span-wise rims are more aligned in the horizontal direction.

Table A7: Near nozzle images for 80% glycerin/water spray atomizing with nozzle N1 at different pressures.

Z(mm)	N1 - 80% glycerin - 500PSI	N1 - 80% glycerin - 700PSI	N1- 80% glycerin - 900PSI
0	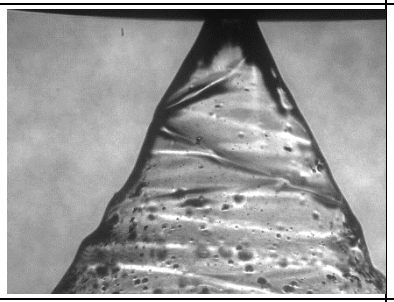	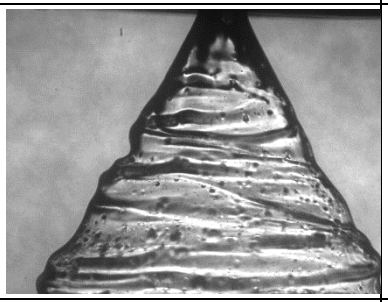	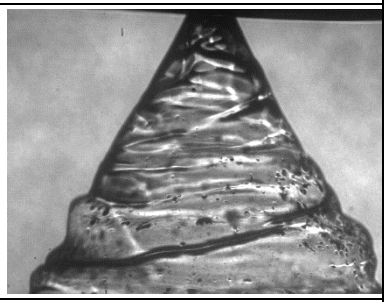
4.98	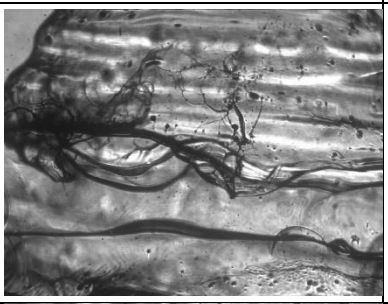		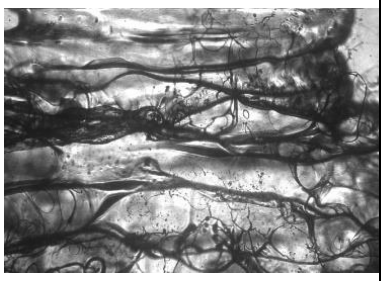
9.96	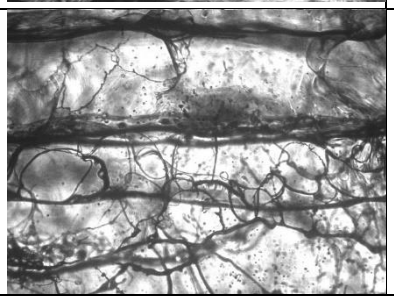	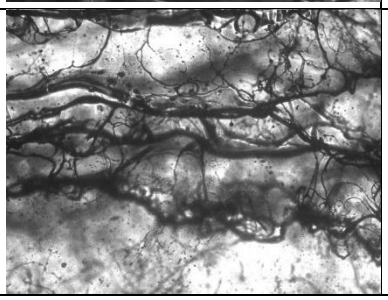	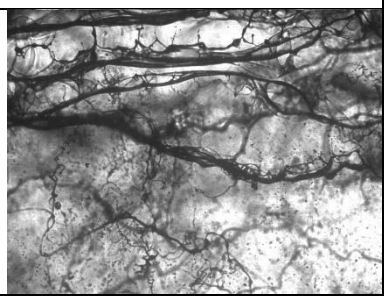

Table A8 shows the images of spray with 0.25% CMC/water solution for atomizing with nozzle N1 at different pressures. Compared to water and 60% glycerin solution, the conical sheet does not perforate until about 6 mm downstream. Compared to 80% glycerin, the sheet is wavier and the wavelength is smaller. The liquid sheet still breaks up due to perforations on the sheet. However, the streamwise ligaments do not break immediately as shown at 9.96 mm downstream for all the cases. There are almost no droplets generated at this position and the streamwise ligaments are stretched and entangled with the spanwise ligaments. It will take longer time for the web of ligaments breaks completely into the droplets.

Table A8: Near nozzle images for 0.25% CMC/water spray atomizing with nozzle N1 at different pressures.

Z(mm)	N1 - 0.25% CMC - 500PSI	N1 - 0.25% CMC - 700PSI	N1- 0.25% CMC - 900PSI
0	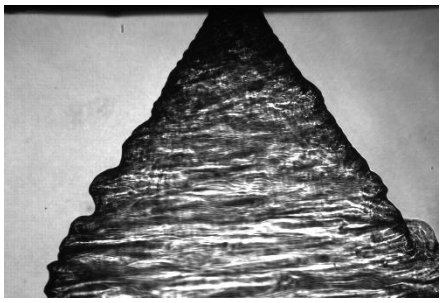	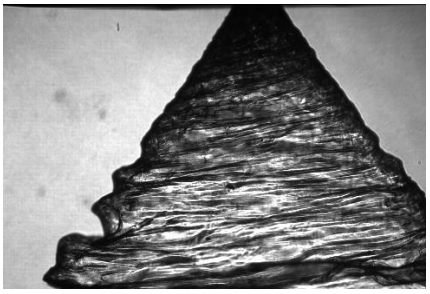	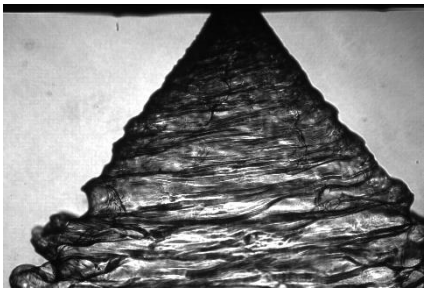
4.98	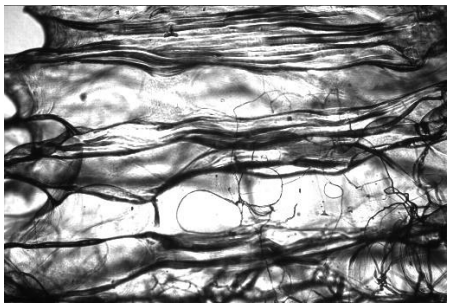		
9.96			

Table A9 shows the images of spray with 0.5% CMC/water solution for atomizing with nozzle N1 at different pressures. Compared to the above-mentioned cases, the injection pressure cannot provide enough inertia forces to counter the viscous force to form a stable air core at the center of the cone. The radius of the cone does not increase proportionally with the distance downstream. This will result in a breakup mechanism in a different regime which is not desired and will generates lots of large droplets (~1mm) as shown in Fig. A2.

Table A9: Near nozzle images for 0.5% CMC/water spray atomizing with nozzle N1 at different pressures.

Z(mm)	N1 - 0.5% CMC - 500PSI	N1 - 0.5% CMC - 700PSI	N1- 0.5% CMC - 900PSI
0	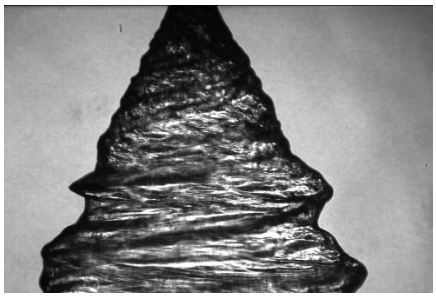	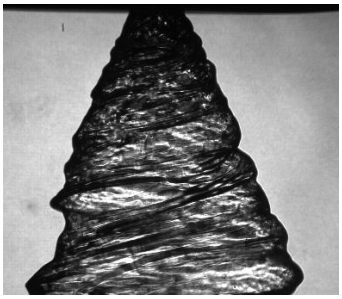	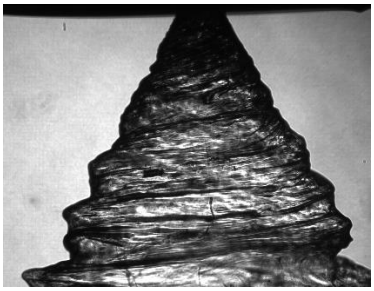
4.98	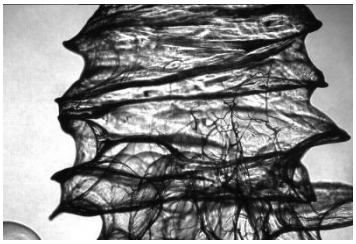		
9.96	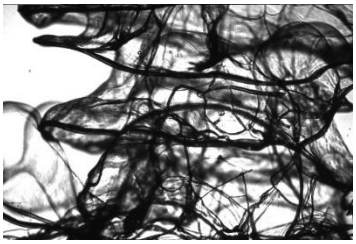		

A.6. Summary

Experiments were performed using two pressure-swirl nozzles with different orifice diameters. Eighteen different operating conditions were tested with high injection pressure (up to 900 psi) and high viscosity fluids (up to 60 mPa.s). The droplet sizes distribution and other statistics were measured using Malvern Spraytec Dropsizer at 80 mm downstream from the nozzle exit. In addition, images at the near nozzle region (within 20mm from the nozzle exit) were taken to study the breakup mechanism of the liquid sheet. The conical liquid sheet was found to break up due to the perforation growth on the thin region between the wave crests of the Kelvin-Helmholtz surface wave. This resulted in a much shorter breakup length compared to the prediction made in the popular LISA model, especially for the high viscosity cases. Two different breakup mechanisms were identified from the near nozzle images: the thick span-wise ligaments generated by the thick wave crests forms large droplets and the thin stream-wise ligaments generated by perforation on thin sheet between wave crests forms small droplets. The mixture distribution with lognormal distributions were found to fit the experimental data best and it made good predictions on the d_{32} of the sprays.

References

Bhatia, J., Domnick, J., Durst, F., & Tropea, C. ,1988. Phase ‐ Doppler ‐ Anemometry and the Log ‐ Hyperbolic Distribution applied to Liquid Sprays. *Particle & Particle Systems Characterization*, *5*(4), 153–164.

Clark, C. and Dombrowski, N., 1972. Aerodynamic instability and disintegration of inviscid liquid sheets. Proceedings of the Royal Society of London. A. Mathematical and Physical Sciences, 329(1579), pp.467-478.

Cousin, J., Yoon, S.J. and Dumouchel, C, 1996. Coupling of classical linear theory and maximum entropy formalism for prediction of drop-size distribution in sprays: application to pressure swirl atomizers. *Atom. Sprays*, *6*, pp. 601-622.

Dombrowski, N. and Johns, W., 1963. The aerodynamic instability and disintegration of viscous liquid sheets. Chemical Engineering Science, 18(7), p.470.

Dumouchel, C, 2006. A new formulation of the maximum entropy formalism to model liquid spray drop-size distribution. Part. Part. Syst. Charact, 23, pp. 468-479.

Dumouchel, C., Yongyingsakthavorn, P., & Cousin, J., 2009. Light multiple scattering correction of laser-diffraction spray drop-size distribution measurements. International Journal of Multiphase Flow, 35(3), pp. 277–287.

Glycerin Producers'Association, 2006. Physical properties of glycerine and its solutions. Glycerine Producers' Association, New York.

Jazayeri, S. and Li, X., 2000. Nonlinear instability of plane liquid sheets. Journal of Fluid Mechanics, 406, pp.281-308.

Kolmogorov A. N. ,1941. On the logarithmic normal distribution law of particles with dimensions of fragmentation. Dok. Acad. Nauk SSSR, 31, 99.

Li, X.; Tankin, R.S, 1987. Droplet size distribution: a derivation of a nukiyama-tanasawa type distribution function. Comb. Sci. Technol. 56, pp. 65-76.

Loustalan, P., Davy, M., and Williams, P., 2003. Experimental Investigation into the Liquid Sheet Break-Up of High-Pressure DISI Swirl Atomizers, SAE Technical Paper 2003-01-3102.

Nukiyama, S. and Tanasawa, Y.,1939. An Experiment on the Atomization of Liquid : 3rd Report, On the Distribution of the Size of Droplets. Trans. Soc. Mech. Eng. Jpn. 5, pp. 131-135.

Park, K., and Heister, S., 2010. Nonlinear modeling of drop size distributions produced by pressure-swirl atomizers. International Journal of Multiphase Flow, 36(1), 1–12.

Schmidt, D.P., Nouar, I., Senecal, P.K., Rutland, C.J., Martin, J.K., Reitz, R.D., 1999. Pressure-swirl atomization in the near field, SAE Technical Paper Series 1999-01-0496.

Sellens, R.W., 1987. Drop Size and Velocity Distributions in Sprays. A New Approach Based on the Maximum Entropy Formalism. Ph.D. Thesis, University of Waterloo, Ontario.

Sellens, R.W. and Brzustowski, T.A, 1985. A prediction of the drop-size distribution in a spray from first principles. Atom. Spray Tech., 1, pp. 89-102.

Sellens, R.W. and Brzustowski, T.A, 1986. A simplified prediction of droplet velocity distribution in a spray. Comb. Flame, 65, pp. 273-279.

Senecal, P., Schmidt, D., Nouar, I., Rutland, C., Reitz, R. and Corradini, M., 1999. Modeling high-speed viscous liquid sheet atomization. International Journal of Multiphase Flow, 25(6-7), pp.1073-1097.

Sindayihebura, D. and Dumouchel, C.,2001. 3. Pressure atomiser: Hole breakup of the sheet. Journal of Visualization, 4(1), 5–5.

Stapper, B., Sowa, W. and Samuelsen, G., 1992. An Experimental Study of the Effects of Liquid Properties on the Breakup of a Two-Dimensional Liquid Sheet. Journal of Engineering for Gas Turbines and Power, 114(1), pp.39-45.

Tratnig, A. and Brenn, G., 2010. Drop size spectra in sprays from pressure-swirl atomizers. International Journal of Multiphase Flow, 36(5), pp.349-363.

Van Der Geld, C.W.M. and Vermeer, H., 1994. Prediction of drop size distributions in sprays using the maximum entropy formalism: the effect of satellite formation. International Journal of Multiphase Flow 20, 363–381.

VILLERMAUX, E. 2007 Fragmentation. Annu. Rev. Fluid Mech. 39, 419–446.

Villermaux, E., Marmottant, P., Duplat, J., 2004. Ligament-mediated spray formation. Phys. Rev. Lett. Vol. 92, Issue 7,pp. 745011-745014.

Vijay, G., Moorthi, N. and Manivannan, A., 2015. INTERNAL AND EXTERNAL FLOW CHARACTERISTICS OF SWIRL ATOMIZERS: A REVIEW. Atomization and Sprays, 25(2), pp.153-188.

Wang, X. F., and Lefebvre, A. H., Atomization Performance of Pressure Swirl Nozzles, AIAA Paper, 1986.

Weber, C., Zum Zerfall eines Flüssigkeitsstrahles. Z. Angew. Math. Mech. 11, 136–154, 1931.

Yongyingsakthavorn, P.; Cousin, J.; Dumouchel, C.; Hélie, J. Piezo-Spray Drop-Size Measurements by Laser-Diffraction Technique in the Presence of Multiple Scattering Effects. In Proceedings of the ILASS-Europe 2008, Paper ID ILASS08-070, Como Lake, Italy, September 2008.

Appendix B - Twin-Fluid Nozzle

B.1. Benchmark data set: Two-fluid nozzles

To best support the analysis in Objective 2, we have focused on planar, external mixing two-fluid nozzles. That is, nozzles where the atomization occurs at the exit plane of the nozzle where it can be easily viewed and imaged. We have chosen the 1/4J external mixing family of nozzles from Spraying Systems Co., as their modular design allows for many nozzle geometries across a wide range of scales. Figure B1 shows the exploded view of this nozzle setup along with the relevant dimensions being controlled. These dimensions are the liquid orifice diameter, D_l, and the gas annulus inner and outer diameters, $D_{g,i}$ and $D_{g,o}$, that determine the gas annular thickness, b_g, which is commonly used in many analyses.

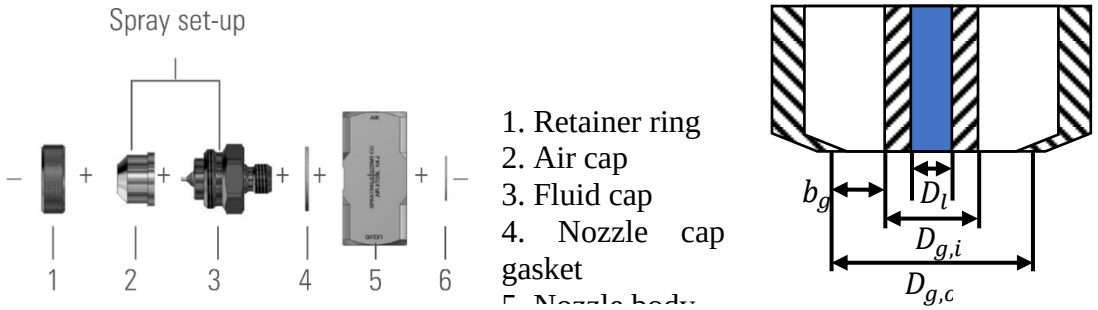

Figure B1: Exploded view and relevant dimensions of Spraying Systems Co. 1/4J external mixing two-fluid nozzle.

The two components that can be changed to alter the nozzle geometry are the fluid cap and air cap. Table B1 tabulates the fluid and air caps used in the present study with their related dimensions, as well as the standard setup configurations recommended by Spraying Systems Co. The 2050 and 2850 fluid caps are representative of typical lab-scale two-fluid atomizers ($D_l < 1$ mm), while the 60100 fluid cap is representative of production-scale two-fluid atomizers ($D_l > 1$ mm). While many nozzle permutations are available, we have focused specifically on the 2050-70 and 2850-70 setups for the lab-scale tests and the 60100-120 setup for the production scale. Comparing these setups allows us to isolate the effect of changing only D_l while keeping b_g constant. D_l is a stronger governing factor as it alters the interfacial area between the liquid and air streams, while b_g primarily serves to change the gas speed for a given flow rate, which is already being controlled directly via the flow rate.

Table B1: Spraying Systems Co. 1/4J external mixing two-fluid nozzle dimensions (in mm) and setups

Fluid Caps	D_l	$D_{g,i}$	Air Caps	$D_{g,o}$	Tested Standard Setups
2050	0.51	1.27	70	1.78	2050-70
2850	0.71	1.27	120	3.05	2850-70
60100	1.52	2.55			60100-120

The testing carried out in this project has captured both the droplet (or particle) size distribution (PSD), as well as near-nozzle images (NNI) and has consisted of three phases: 1. Water tests as

the baseline inviscid fluid, 2. Aqueous glycerin mixtures as a baseline for viscous fluids, and 3. Aqueous polymeric fluids, consisting of PEG 4000 (a viscous Newtonian polymer) and CMC (a shear-thinning non-Newtonian polymer). The tested mixture ratios and their viscosities are tabulated Table B2.

Table B2: Fluid viscosities

	Fluid	Wt.%	Viscosity [mPa.s]
Baseline inviscid	Water		1
Baseline viscous	Glycerin (aq.)	60	12
		85	148
		90	213
Newtonian Polymer	PEG 4000 (aq.)	20	6.2
		30	14.2
Non-Newtonian Polymer (shear-thinning)	CMC (aq.) [1]	0.25	>20-15
		0.5	>40-30

Note that the viscosities of the CMC mixtures are the expected viscosities based on ref. [1]; however, testing performed in the Rheology Laboratory and the University of Toronto using similar equipment have not provided results consistent with ref. [1]. The tested values suggest a Newtonian behaviour and a much lower viscosity. The measurements indicate a Newtonian behaviour with a considerably lower viscosity than expected; however, our spray testing indicates that the CMC mixtures behave as if they have a much higher viscosity, even than that reported by [1], similar to that of the 85% glycerin mixture. This can be seen in Figure B2, where the sprays of water, 60% glycerin, 85% glycerin, and 0.25% CMC mixtures are compared.

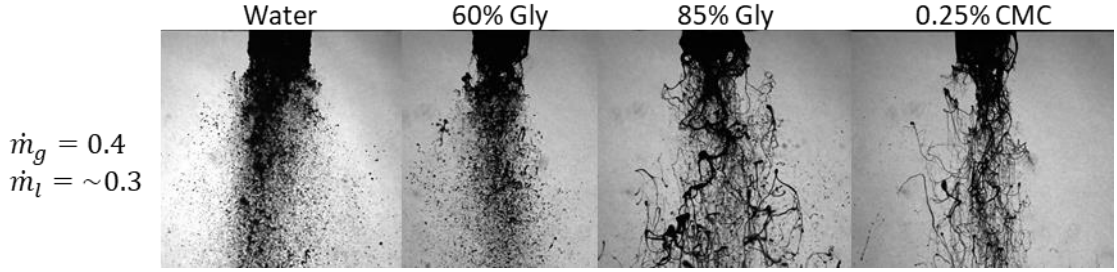

Figure B2: Comparison of water and glycerin mixtures to 0.25% CMC mixture

The more viscous the spray is, the more pronounced the ligaments become. If the CMC mixture really had a viscosity closer to that measured or reported in [1], then it would be expected to behave similarly to the 60% glycerin mixture; however, it clearly behaves more like the much more viscous 85% mixture. We suspect this is due to the CMC mixture exhibiting a much higher extensional viscosity, which would not be apparent in the measurement method implemented in [1] or in our own rheology measurements. We are still working to find an accessible measurement of the extensional viscosity to verify our theories.

Although previous studies have focused typically on mean spray statistics, such as the Sauter Mean Diameter (SMD), a significant drawback of these statistics is that they do not describe the distribution of the spray, particularly, it's modality. Real-world sprays, especially viscous ones, produce wide, multi-modal distributions. Although the SMD can provide a reasonable prediction of some trends, it does not tell the full story of the spray distribution.

NNI's of the glycerin mixture sprays at two selected conditions (one at low flow rates and one at high flow rates) using the pilot-scale (2850-70) and production scale (60100-120) nozzles are shown in Figure B3 and Figure B4, respectively.

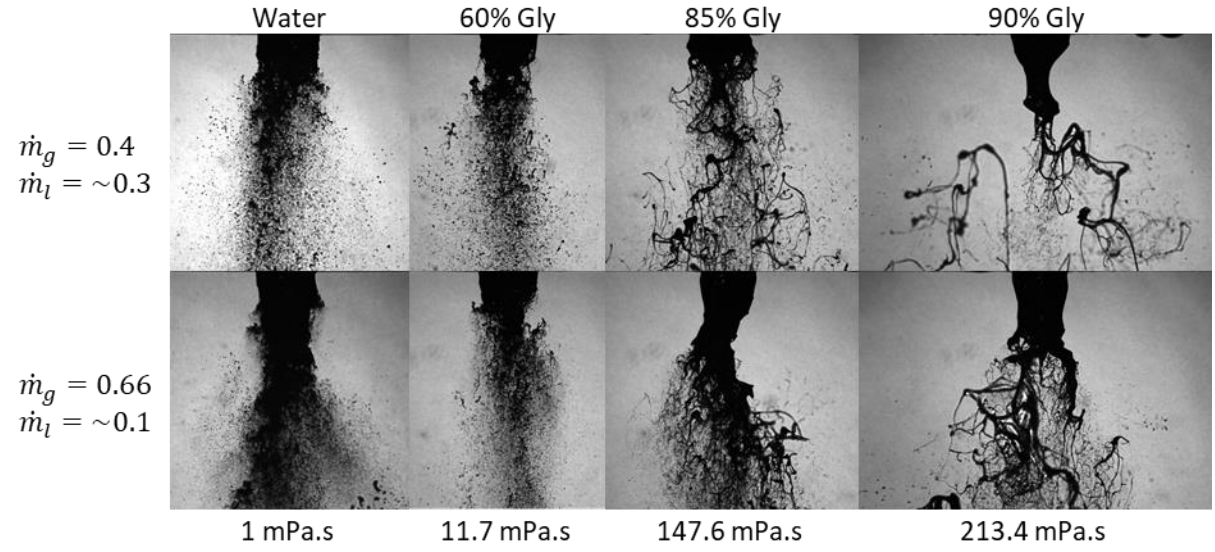

Figure B3: Images of pilot-scale spray for water and glycerin mixtures at low (top) and high (bottom) flow rates.

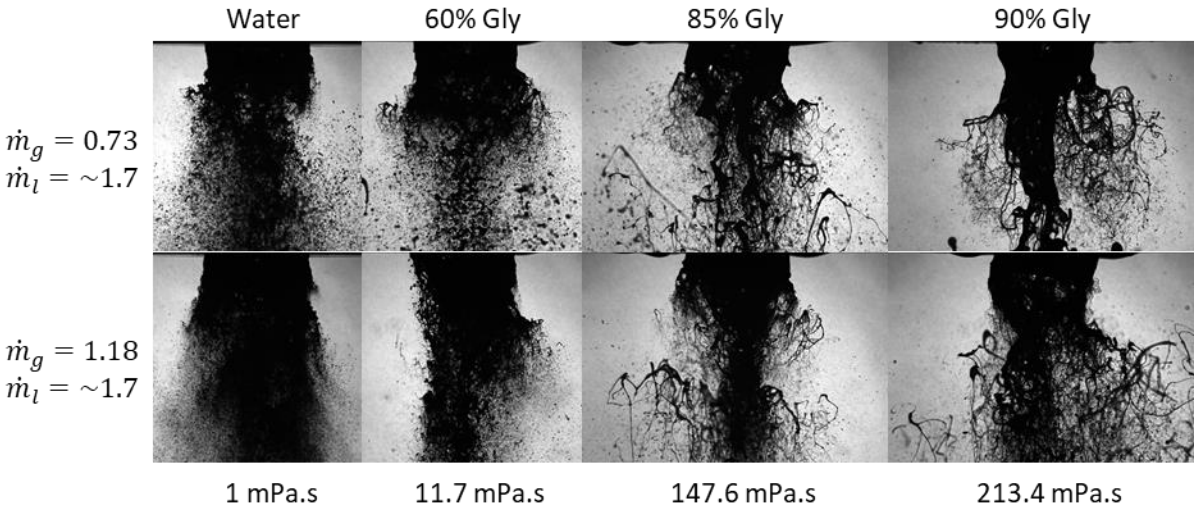

Figure B4: Images of production-scale spray for water and glycerin mixtures at low (top) and high (bottom) flow rates.

The measured PSDs for the water and glycerin mixtures at varying flow conditions using the pilot-scale (2850-70) and production scale (60100-120) nozzles are shown in Figure B5 and Figure B6, respectively.

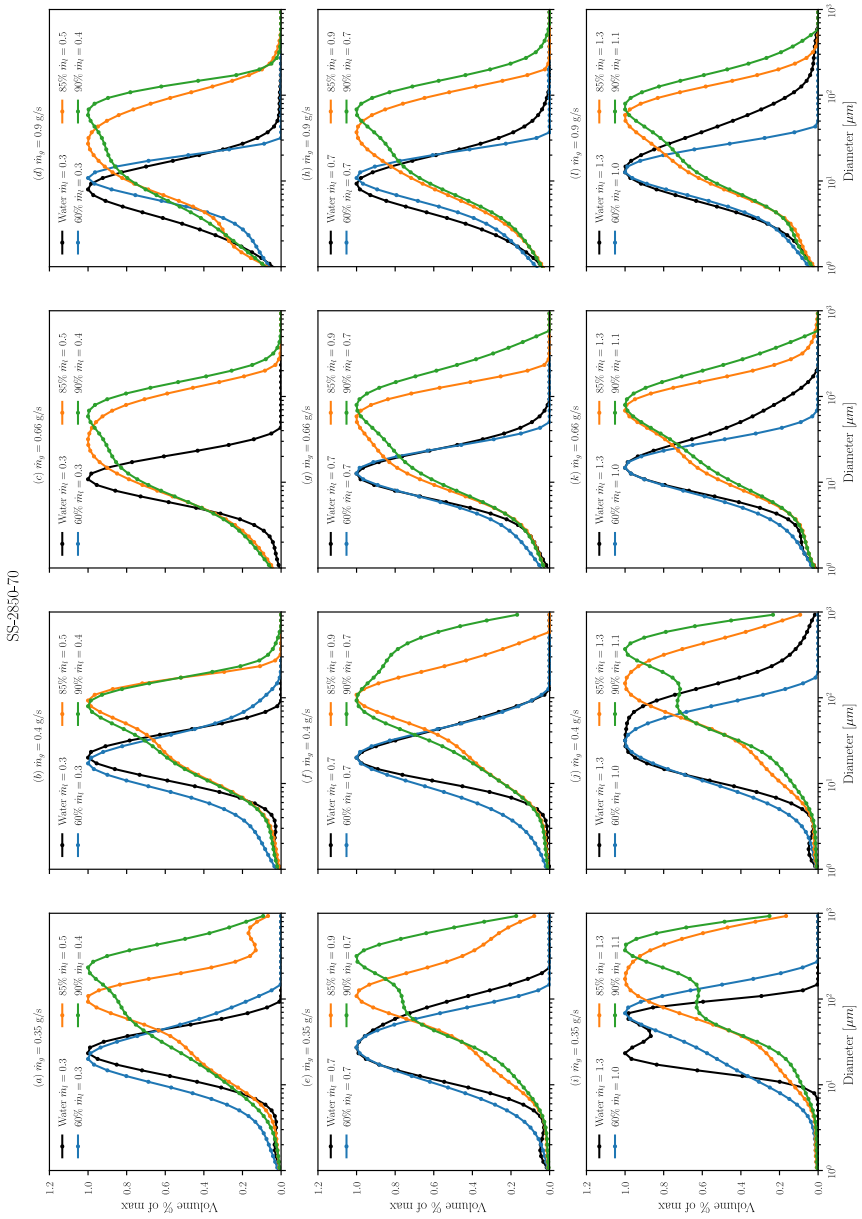

Figure B5: PSDs for water and glycerin mixtures at varying flow rates for pilot scale nozzle

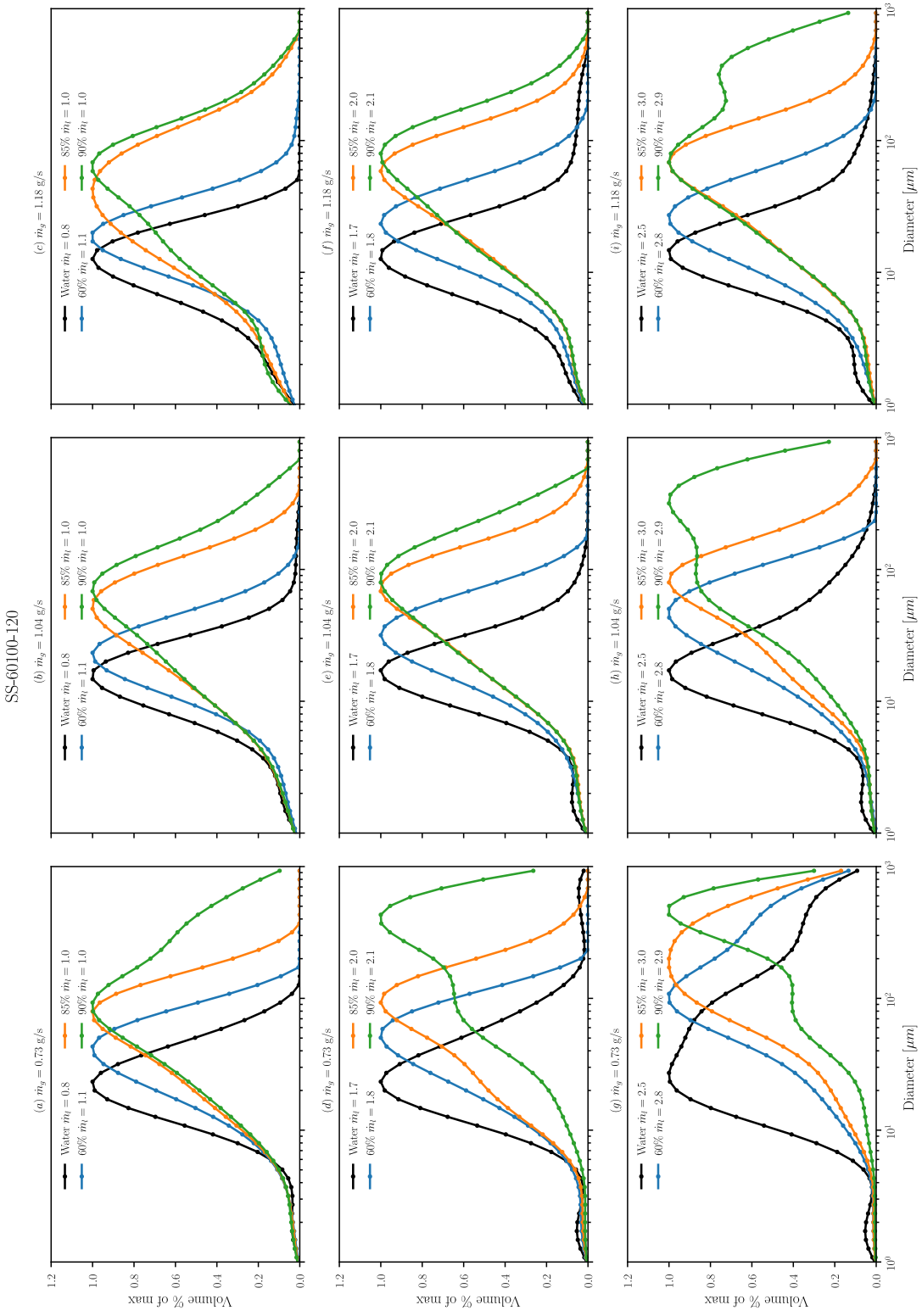

Figure B6: PSDs for water and glycerin mixtures at varying flow rates for production scale nozzle

B1.1 Measurement of ligament sizes

In addition to acquiring the PSD of the droplets from the spray, the NNI's were collected to provide a visualization of the atomization process, as well as to provide an opportunity to measure the ligaments that are prevalent in viscous sprays. While we had hoped to develop automated image processing algorithms to provide an extensive characterization of the ligaments, attempts to do so were not successful due to the complexity of the ligament networks. As a first step towards quantifying the ligament sizes, we have measured their thicknesses manually from images, randomly selecting ligaments and locations on them at which to take the measurements across 200 images. Such a measurement campaign is very time intensive, thus the same measurements for other liquids and nozzles are still in progress. The results of the ligament measurements for the water (inviscid) base case at varying gas and liquid flow rates for the 2850-70 nozzle are presented in figure below. Although these measurements are for an inviscid fluid at low gas flow rates, these conditions provide a dynamically similar spray to the more viscous case and provide a good basis for comparing our theoretical models for the formation of the ligaments independent of the viscous effects. Note that we have independently measured the ligaments generated immediately at the surface of the liquid jet, as well as those that result from the breakup of the bulk of the liquid jet. The ligaments generated at the surface of the jet are typically smaller than those generated in the breakup of the bulk of the jet.

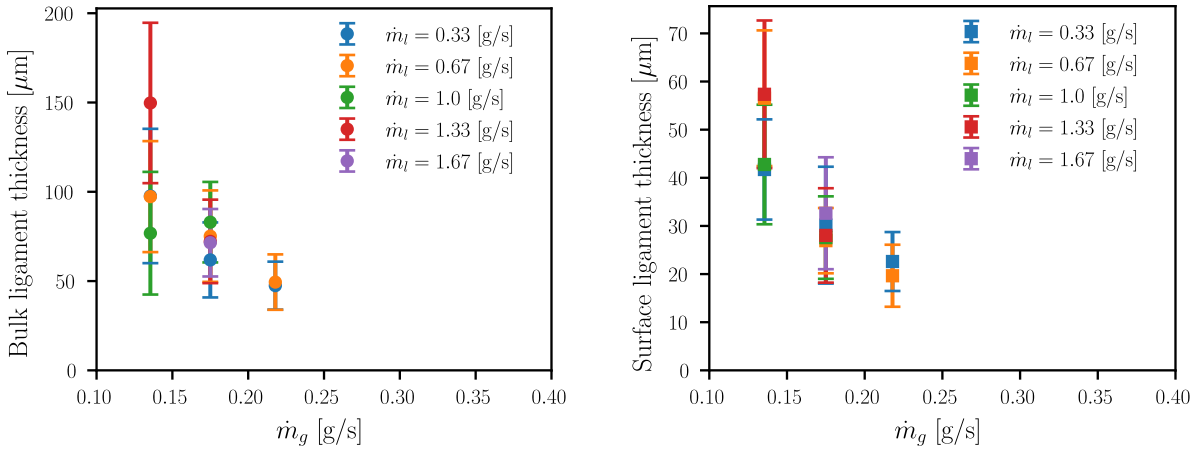

B.2. Correlations for nozzle scaling, size distribution

When developing correlations for sprays, it is important for the correlation to consider the phenomenology of the spray. One of the key factors for developing correlations for two-fluid atomization, therefore, is the morphology of the spray, which depends on the operating conditions of the nozzle. While various researchers classify these morphologies differently, the two morphologies of interest in the present work are membrane-type breakup and fiber-type breakup [2], which are shown in Figure B7.

Membrane-type breakup

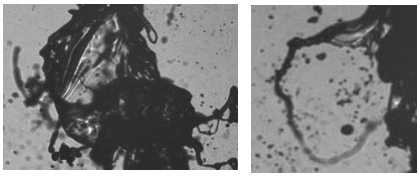

Fiber-type breakup

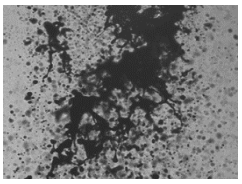

Figure B7: Example images of membrane- and fiber-type breakup

Previous studies have shown empirically that the breakup morphology can be categorized in terms of the Weber number (We) and the Ohnesorge number (Oh) [2,3]. We number describes the competition between the flow inertial and the surface tension forces, while Oh relates the viscous forces to the same. Fiber-type breakup occurs at higher We than membrane-type breakup, although as Oh increases, the We at which this transition occurs increases, as higher aerodynamic forces are required to overcome the damping viscous forces.

$$We = \frac{\rho_g U^2 d_0}{\sigma}, \qquad Oh = \frac{\mu_l}{\sqrt{\rho_l \sigma d_0}},$$

The existing analytical models for two-fluid atomization are focused on the fiber-type breakup morphology [4,5] as this morphology typically provides the smallest droplet sizes and a mono-modal droplet size distribution. However, for very viscous fluids, this morphology is not easily attainable as the gas velocities required are supersonic. Achieving these conditions requires specialized nozzle geometry and a very high consumption rate of the atomizing gas. No analytical models exist for the membrane-type breakup morphology, even for low viscosities. Importantly, the existing models do not predict the formation of the ligament networks characteristic of these types of breakup. This is further complicated by the need for the prediction of the size distribution, as the existing models are based only on one mechanism in the breakup, which in turn gives only a single size prediction that is typically related to the SMD. To model the distribution of the breakup, particularly for multi-modal distributions, multiple modes and mechanisms of breakup must be considered. This is evident in Figure B8 and Figure B9, where the sprays for varying glycerin mixtures (varying viscosity) are compared. The water and 60% glycerin cases exhibit similar morphologies (fiber-type breakup), which result in similarly shaped PSDs, while the 85% and 90% glycerin mixtures show a different morphology (membrane-type breakup), and exhibit much wider and multi-modal distributions.

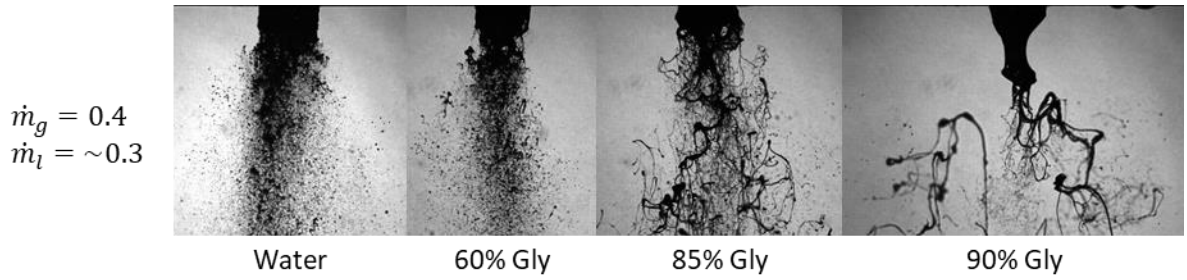

Figure B8: images of sprays at varying viscosities. Water and 60% glycerin solutions exhibit a similar morphology to each other, while the 85% and 90% glycerin mixtures exhibit a different morphology.

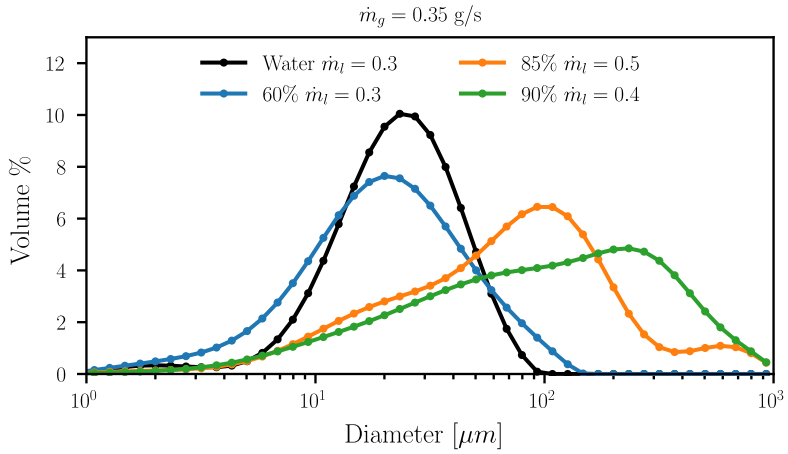

Figure B9: Size distributions for the cases in figure 3.

The two-fluid atomization process has been likened to the breakup of droplets in a high-speed airflow, which also exhibit various morphologies with We and Oh, such as bag or membrane-like morphologies at low We. Many of the existing analytical models for sprays use droplet breakup models to handle the breakup of the surface waves that form on the liquid jet [4,5], however droplet breakup modelling is also limited to the high We morphologies [6,7] which do not relate to the membrane-type morphology of interest in high viscosity atomization where ligament networks are formed. To formulate an analytical model for the breakup of a high-viscosity jet, it is therefore necessary to first model the breakup of inviscid drops and sprays in a way that models the formation of the ligament networks, and how the generated ligament networks break by a variety of mechanisms.

Therefore, the steps for the development of the two-fluid spray correlation are as follows:

1. Develop a model for inviscid droplet breakup, focusing on bag-type morphologies
    a. Formation of ligaments
    b. Breakup of ligaments into a distribution of sizes
2. Modify the droplet model for the geometries of inviscid two-fluid spray atomization
3. Modify the spray model to incorporate:
    a. High viscosity
    b. Elevated temperatures

B.2.1. Droplet breakup

B.2.1.1 Ligament formation

In our paper "On aerodynamic droplet breakup" [8], we presented a detailed study of the dynamics that lead to the ligament formation in droplet breakup. We showed how the initial expansion of the windward droplet face follows a linear relationship modelled by

$$\frac{\dot{d}}{d_0} = \frac{1.125}{\tau}\left(1 - \frac{32}{9We}\right).$$

This expansion of the windward droplet face results in the formation of a windward disk in front of an undeformed core. The windward disk goes on to form the rim and bag, while the undeformed core may go on to form a stamen or undergo its own breakup following the breakup of the windward disk. The expansion rate of the windward disk, in addition to a balance with the surrounding air flow, results in it forming a rim of thickness

$$\frac{d_i}{d_0} = \frac{4}{\frac{\rho_l \dot{d}^2 d_0}{4\sigma} + 10.4} - 0.05.$$

The windward disk, consisting of the peripheral rim (1) and the thinned sheet (2), and the undeformed core (3) are shown in Figure B10.

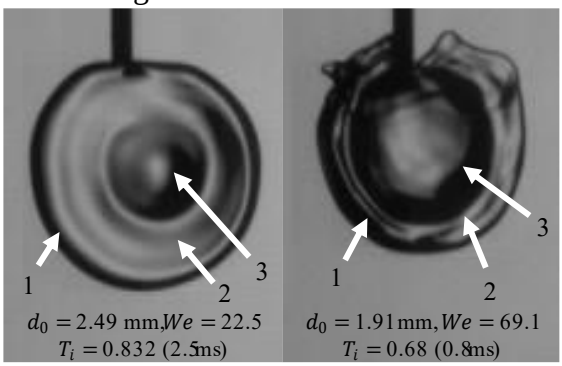

Figure B10: Images of the structures formed in the initial deformation stage for bag and stamen (left) and multibag (right) breakup, showing the rim (1), thinned sheet (2), and core (3).

The rim goes on to form the dominant ligament in the breakup, while the thinned sheet becomes the bag(s). If the core undergoes its own breakup, as in multi-bag or sheet-thinning breakup, it may also form ligaments. Based on the prediction of the rim thickness, the volumes of the windward disk and undeformed core can also be predicted, which are related to the morphology of the droplet breakup. As the bag grows inside of the rim, the bag forces the rim to expand. As the rim expands, it thins to conserve its volume, where the final thickness of the rim will govern the sizes that it breaks into. The bag growth was modelled considering a force balance on the bag tip and was related to the expansion of the rim from the time it was formed to the time it breaks. The nature of the relationship was assumed to be related to the morphology; however, since the work modelled the morphologies as discrete steps instead of continuous transitions, it is simpler to consider an average rim thinning ratio of $d_i/d_f \approx 1/0.64$. Assuming that the rim breaks by the Rayleigh-Plateau capillary instability mechanism, an assumption commonly used in the literature, the rim child droplet size will be given by

$$\frac{d_c}{d_0} = 1.89\frac{d_f}{d_0} = 1.89\left(\frac{d_f}{d_i}\right)\left(\frac{d_i}{d_0}\right).$$

The result is compared to the experimental measurements of the mean rim droplet sizes in Figure B11.

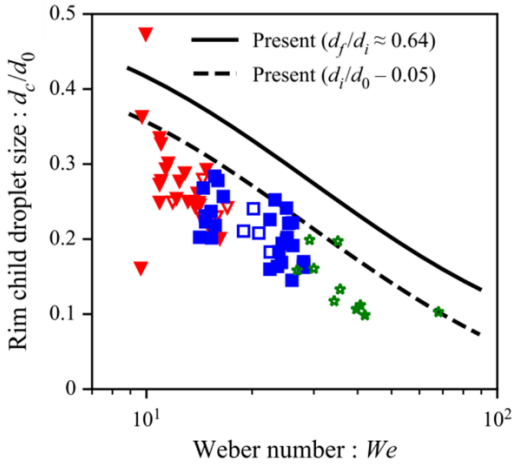

Figure B11: child droplet size vs We in droplet breakup

The results show reasonable agreement to the experiments; however, the prediction is somewhat high. This is due to the assumption that the Rayleigh-Plateau mechanism governs the rim's breakup, as shown in Figure B12. The primary focus of this paper was to model the formation of the rim ligament, which was done successfully. The other mechanisms at play in the breakup of the droplet are discussed in the following section. Note that the factor -0.05 in the equation for d_i/d_0 is an empirical correction for the air-flow separation in the wake of the deformed droplet.

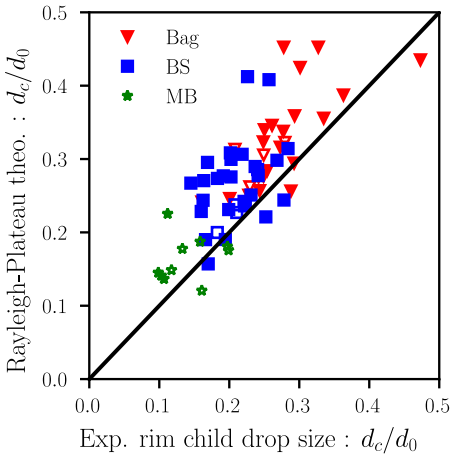

Figure B12: Comparison of the theoretical Rayleigh-Plateau breakup prediction of the rim to the experimental measurements.

B.2.1.2. Ligament breakup and size distribution

In our upcoming work, currently being prepared for submission to the Journal of Fluid Mechanics, we have extended the model for the formation of the rim ligament to include a plethora of breakup mechanisms, each of which contribute to the breakup, with the aim of

predicting for the first time the resulting size distribution of the spray. The main questions addressed in this work are 1. What are the main mechanisms of breakup for the various structures in the droplet, 2. What is the source of variation in these mechanisms that leads to a distribution of sizes, and 3. How can models of these mechanisms be combined to provide a prediction of the overall droplet size distribution.

There are three main geometries that form in droplet breakup that are considered: 1. The nodes that form on the rim of the drop, 2. The bag, and 3. The rim that remains after the nodes have formed.

The nodes that form on the rim are shown in Figure B13. In a previous work [9], the nodes were assumed to form by the Rayleigh-Taylor acceleration instability, and a prediction was made for the number of nodes formed but not the size of the nodes.

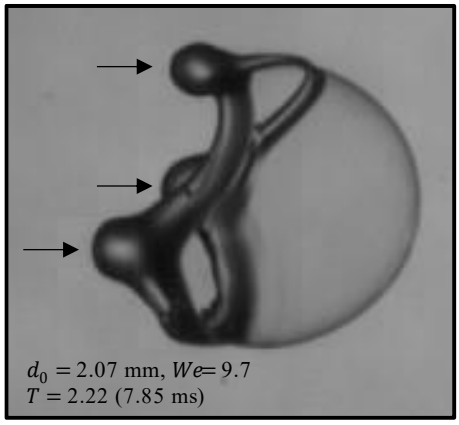

Figure B13: Image of nodes forming on the rim of a droplet undergoing breakup.

In our work, we compared this theory to the Rayleigh-Plateau capillary instability. In these analyses, the previous prediction of d_i/d_0 is used to estimate the rim dimensions at the time the instability takes hold. The two instability theories were found to give comparable results in terms of the predictions for both the number of nodes formed, as well as the resulting size of the droplets. The variation in the node sizes that can form was attributed to local effects that cause more or less of a segment of the rim to flow into the node, rather than remain in the rim. This factor was defined as the node-disk volume fraction, n, defined as the volume fraction of the windward disk that ultimately ends up in the node, and ranges from $n = 0.2 - 1$ with a mean value of $n = 0.4$. The prediction of the node sizes using the Rayleigh-Taylor and Rayleigh-Plateau theories are compared to the experimentally measured node child drop sizes in Figure B14.

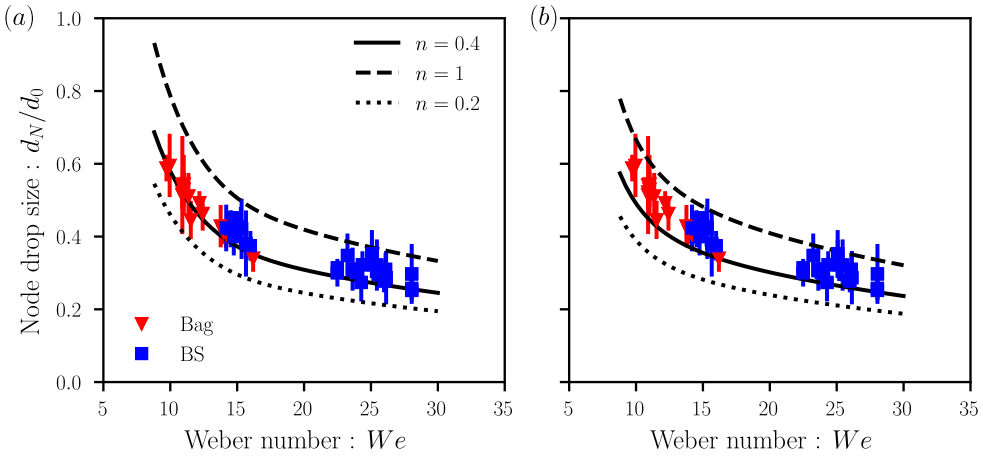

Figure B14: Rayleigh-Taylor (a) and Rayleigh-Plateau (b) predictions for the node child drop size.

The breakup of the bag is difficult to study as its dynamics span over a wide range of scales. The whole bag may form a bubble on the scale of mm, while the bag may have a thickness on the scale of μm, with its breakup taking place in ms, all while the entire drop moves over a few cm. This multi-scale characteristic makes the process difficult to image in a way that all relevant measurements can be made; in particular, the droplets resulting from the breakup of the bag. For this reason, the breakup is described mainly qualitatively, with some modelling used to estimate the characteristic sizes in its breakup. Images of the bursting bag are shown in Figure B15.

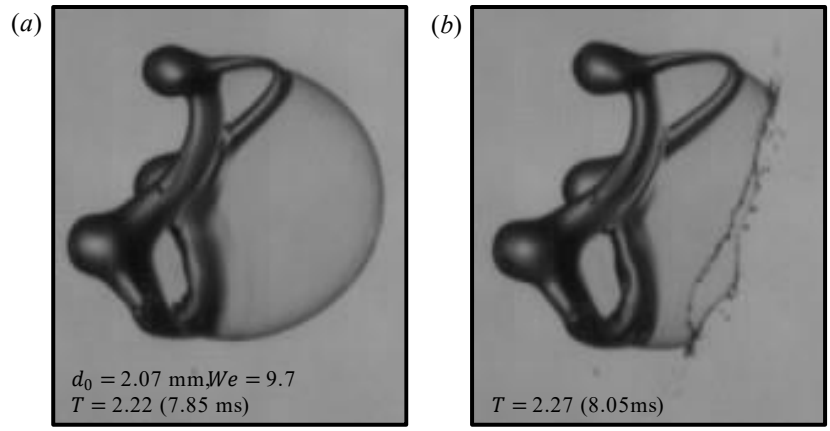

Figure B15: images of the bursting bag

The model of [10], developed for the bursting of static surface bubbles, was found to match the dynamics of the bag very well in terms of its recession speed and the instability at the rim that forms at the perforation of the bag. Using this model, the minimum bag thickness was estimated to be $h_{min} = 2.3 \pm 1.2\ \mu$m. The other relevant sizes in the breakup are the rim thickness, estimated by the model of [10], and its breakup due to capillarity.

As mentioned previously, the breakup of the remaining rim has been assumed to be due to the Rayleigh-Plateau instability; however, this assumption leads to an over-prediction in the average size of the rim drops. By carefully analyzing the breakup phenomenology, we discovered that an additional mechanism in the breakup of the rim is the collision of the receding rim of the bag, as shown in Figure B16.

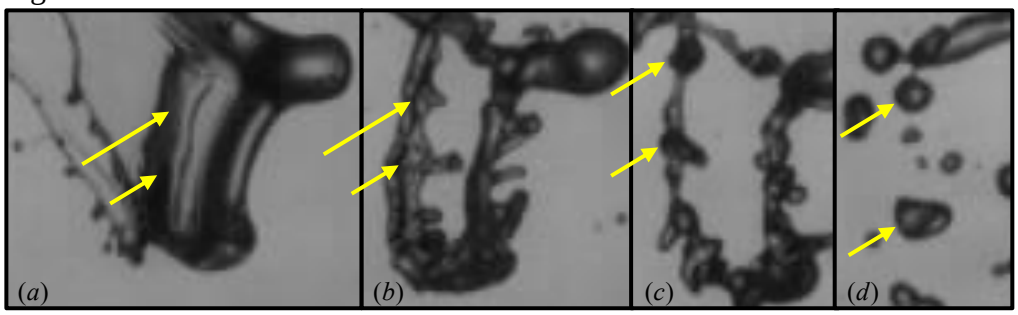

Figure B16: Images of the collision of the receding rim with the main rim of the drop

Since the receding rim is heavily corrugated owing to its own instability, as described previously, it imparts an unequal impulse on the rim, effectively forcing it to break at the same wavelength as the receding rim instability. Variation in this mechanism arises from different collision angles with the rim, which cause the effective imparted wavelength to be longer. At very high collision angles, the force of the collision is insufficient to dominate over the capillary Rayleigh-Plateau mechanism, and so Rayleigh-Plateau breakup can also occur in the breakup of the rim. Figure B17 shows how this variety of mechanisms leads to wide range of breakup sizes, where the Rayleigh-Plateau prediction gives the upper limit of the breakup sizes, the collision mechanism approximately follows the mean sizes, and the satellites resulting from the collision mechanism estimate the lower limit of the breakup sizes of the rim.

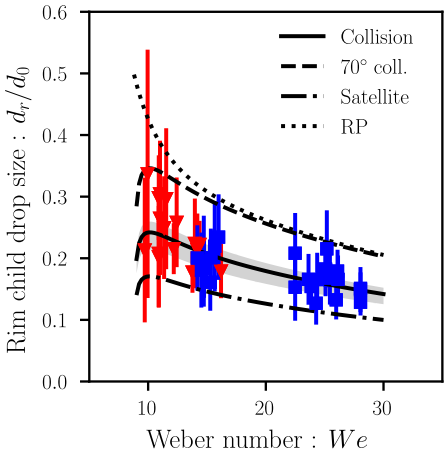

Figure B17: Rim child drop sizes from a variety of mechanisms

The distribution of sizes resulting from breakup is assumed to come from a combination of all of these mechanisms as well as the subtle variations within each mechanism. These mechanisms are are grouped in terms of the primary modes of the breakup (i.e. the geometries within the deformed droplet) such that the overall distribution is the result of the sum of the modes, which

can lead to a multi-modal distribution. While the volume weighting of each mode is determined by models for the volume estimation of each geometry, the relative number weighting of the mechanisms within each mode are assumed to vary as a two-parameter gamma distribution function where the parameters are estimated based on the mean and standard deviation of the predicted sizes for each mechanism within the mode.

In Bag breakup, there are three modes resulting from the rim nodes, the remaining rim, and the bag. The ranges of sizes given by the mechanisms for each of these modes is shown in Figure B18 (a). The resulting combined distribution using the analytical weightings is given in Figure B18 (b). While the location and width of the peaks are reasonably matched by the predicted distribution, the height of the peaks is not so well predicted. This is likely because the particular case being compared is near the transition to the Bag and Stamen morphology, where the breakup may exhibit the `twin-bag' transitional morphology in which a fold appears across the bag dividing it in two owing to the slightly larger mass at the center of the bag due to the small, undeformed core. While this fold primarily affects the bag, it may also have an influence on the rim; in particular, the formation of additional nodes on the rim where it is met by the fold of the bags. The presence of this fold then changes the assumed dynamics of the rim, and thus may reduce the remaining rim's volume more than presently predicted. Figure B18 (c) shows the result using fitted weights, with much better agreement. A better understanding of the transitional behaviour between the morphologies will lead to a better prediction at these conditions.

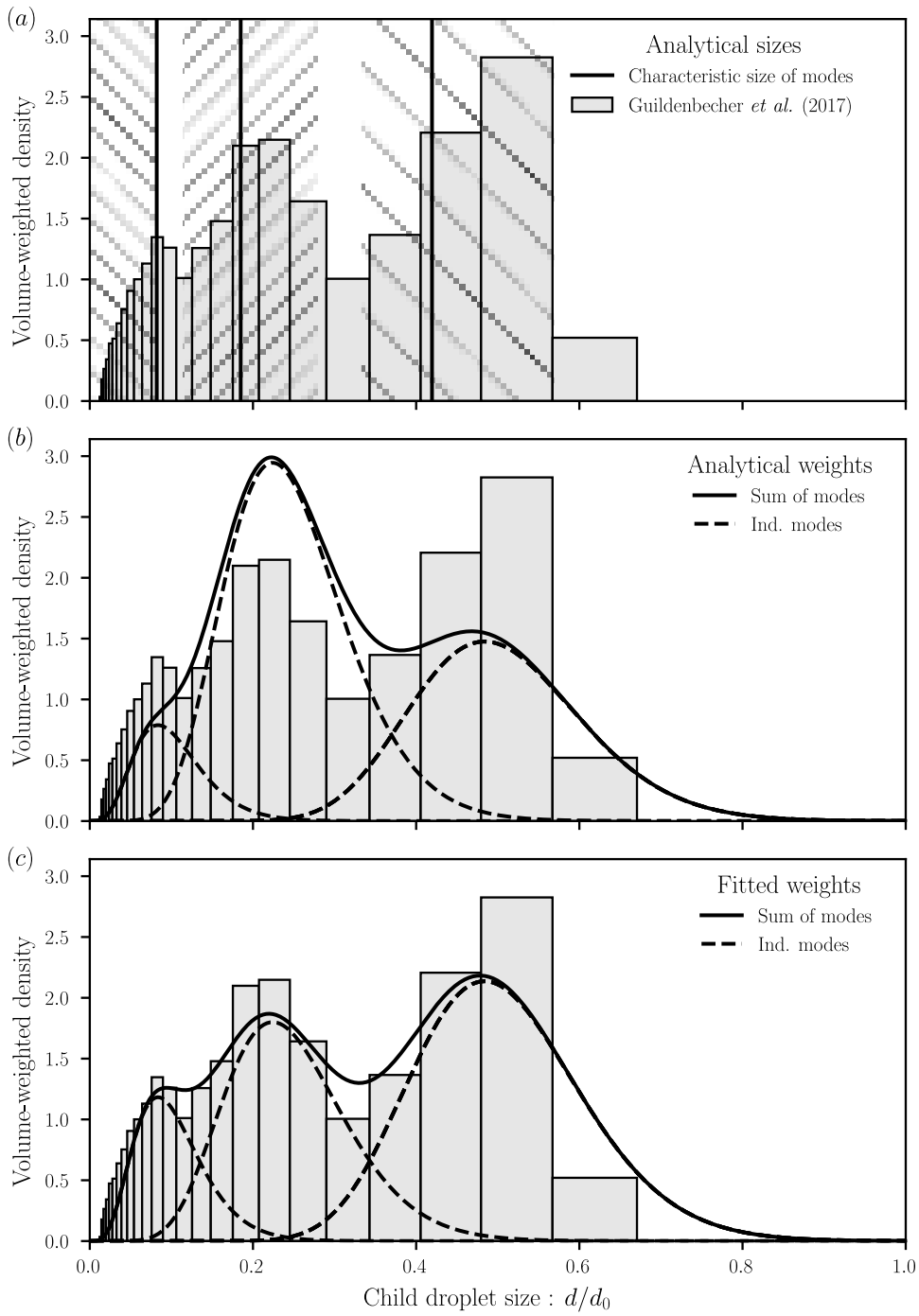

Figure B18: Comparison of distribution prediction to experiments [11] for bag breakup

In multibag breakup, there is the addition of the breakup of the undeformed core, which itself breaks into an additional three modes. Figure B19 (a) shows the resulting distribution considering all six modes of the breakup. Notably, the contributing volume of the bag appears to be over-predicted. This is likely due to the folds between the azimuthal bags being neglected.

The folds between the azimuthal bags leave behind ligaments after the rupture of the bags, which result in sizes similar to the breakup of the rim. As a result, some of the mass of the bag breaks into sizes similar to those of the rim breakup. Since this effect is neglected, the smallest sizes due to the breakup of the bag are over-predicted, while the sizes near the characteristic size of the rim breakup are under-predicted. A better understanding of the dynamics of the bag that lead to the formation of the azimuthal ligaments is needed to improve the present prediction.

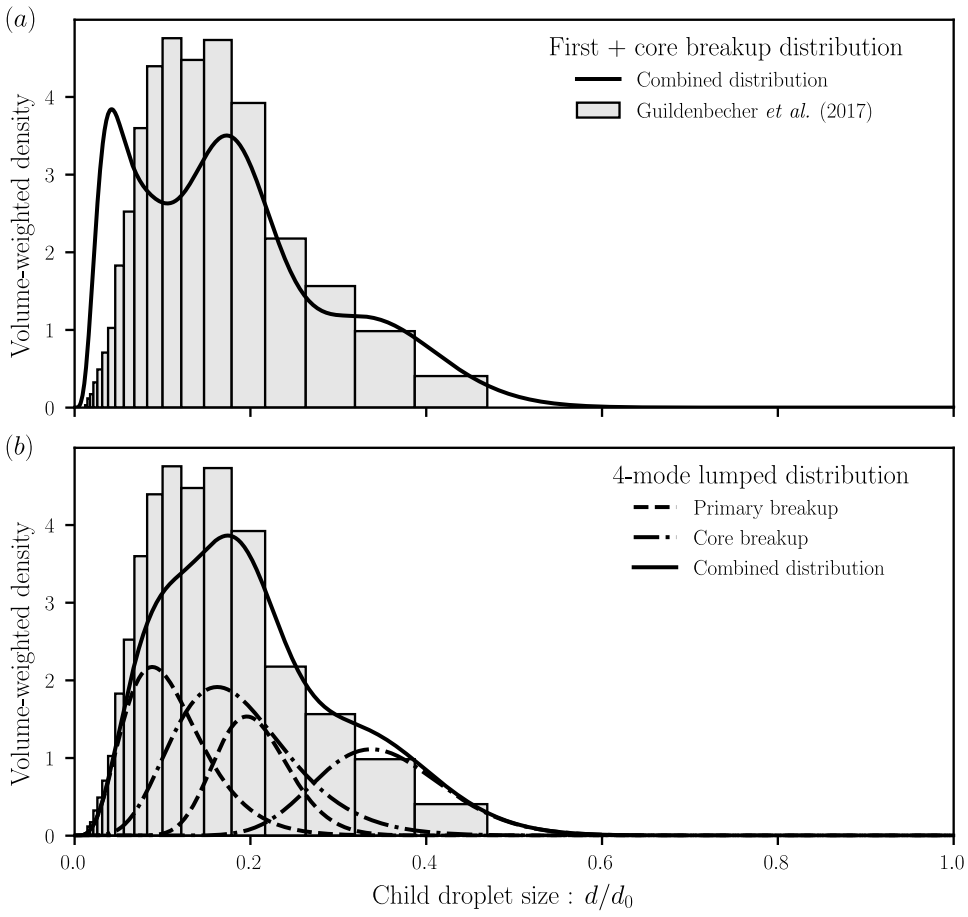

Figure B19: Comparison of distribution prediction to experiments [11] for multi-bag breakup

In multi-bag breakup, several of the modes overlap such that they appear to be monomodal. When this occurs, the weighted mean and standard deviation of the mechanisms contributing to each mode can be used to determine a lumped distribution that captures the overlapping modes as one. This is shown in Figure B19 (b), where the bag and rim modes for both the first and core breakups are lumped together. Since the volume weighting between the bag and rim is what caused the earlier deviation when the modes were treated separately, lumping the modes together somewhat negates this effect.

Figure B20 gives a flowchart of the calculation of the multi-modal distribution.

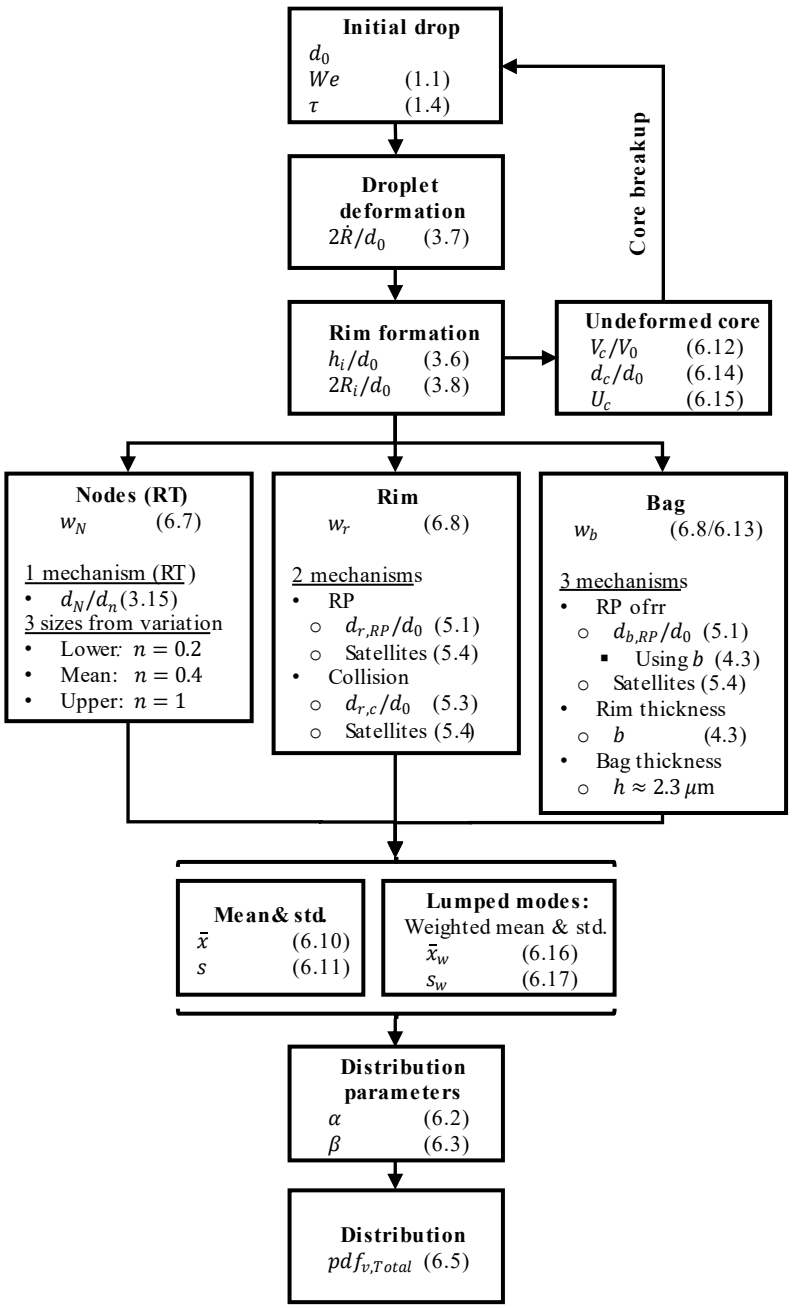

Figure B20: Flowchart of distribution calculation

B.2.2. Extension to two-fluid spray geometry

To extend the droplet breakup models to two-fluid sprays, we first identify the similar geometries that occur in the breakup. Previous works have primarily considered only the varicose surface waves on the liquid jet; however, in practical sprays, the surface waves grow until they start to couple, forming sinuous bulk waves in the liquid jet. Both geometries are susceptible to breakup, as shown in Figure B21.

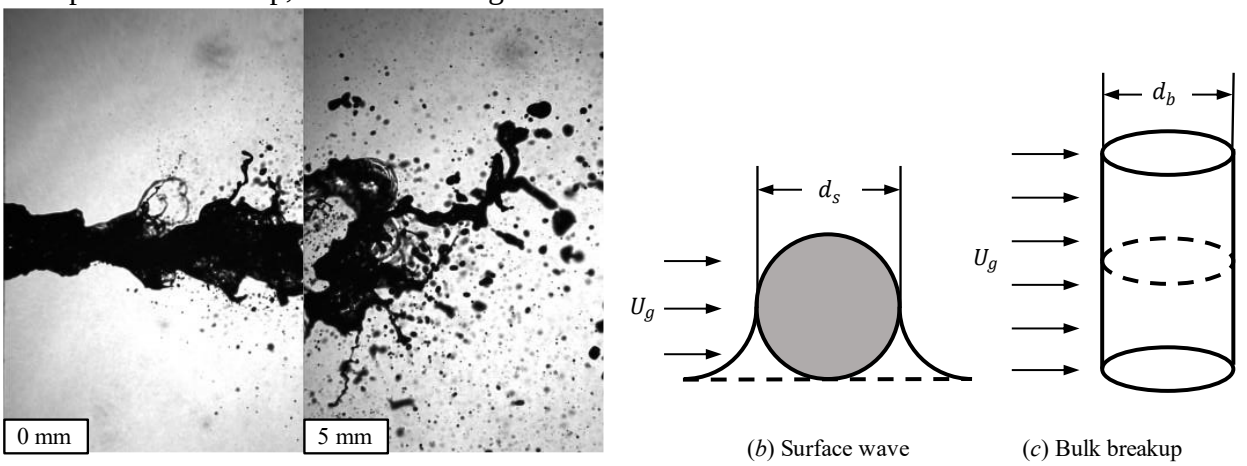

(*a*) Image of spray (*b*) Surface wave breakup geometry (*c*) Bulk breakup geometry

Figure B21: image of spray showing surface and core breakup, and illustrations of the surface wave and core breakup geometries.

The breakup of these geometries is modelled, as a first approximation, by the same model developed for the atomization of a liquid droplet. For the core breakup, the diameter of the liquid jet as it waves into the air flow is assumed to be the diameter of the equivalent droplet. The droplet breakup model for the prediction of the ligament size and characteristic breakup size is compared to the experimental measurements in Figure B22.

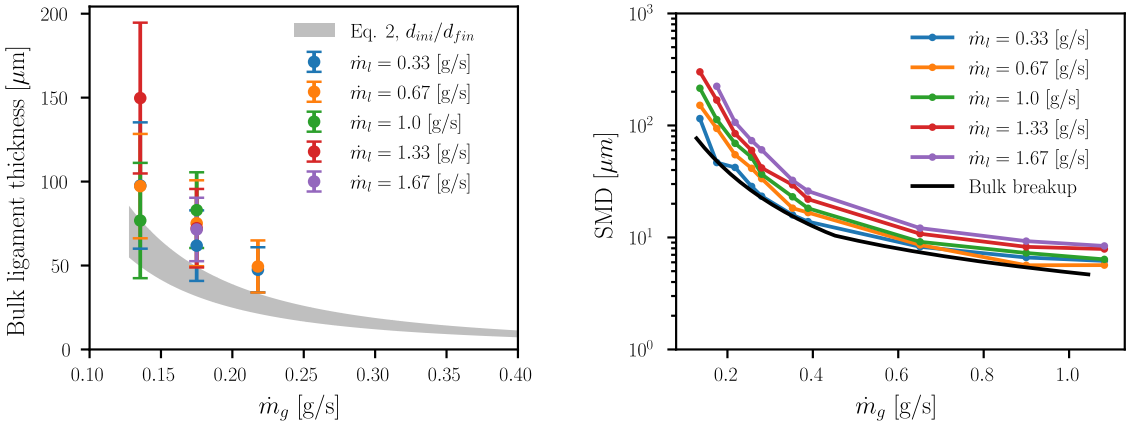

Figure B22: (left) comparison of bulk ligament thickness to theory. (Right) comparison of droplet breakup model for bulk breakup to SMD for varying flow conditions.

The trends and magnitudes in both are found to compare well; however, the effect of increasing liquid flow rate is not predicted by the model. To understand these effects, the PSD must be considered, as in Figure B23. Figure B23 shows how the modality of the distribution affects the

SMD. Since the current prediction only considers the one breakup mechanism, it does not capture the larger mode that grows as the liquid flow rate increases. The bulk breakup prediction, however, does give a good prediction of the lower mode in the PSD.

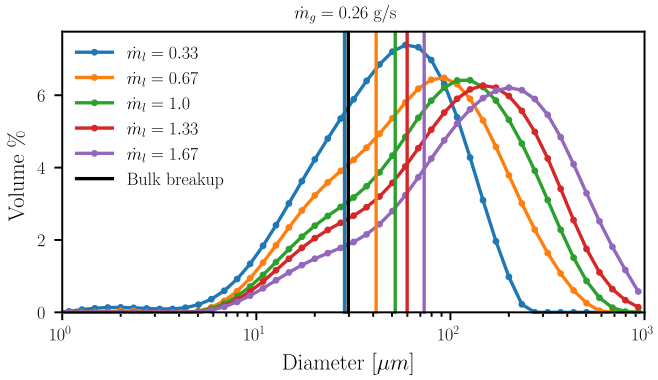

Figure B23: PSD and SMD comparison for varying liquid flow rate.

The larger sizes are believed to come from an intermittency in the breakup of the liquid core, due to the way it waves in and out of the airflow, as shown in Figure B24. This essentially relates to an incomplete breakup of the liquid jet due to insufficient aerodynamic forces, which occurs commonly in highly viscous sprays. This is expected to be modelled similarly to the breakup of the undeformed core in droplet breakup.

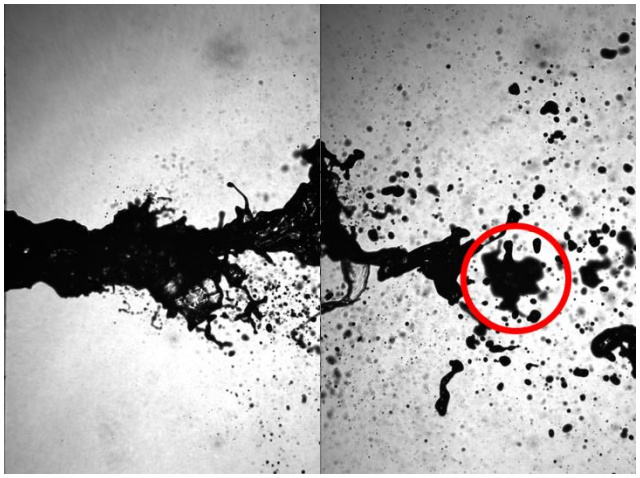

Figure B24: Images showing the intermittent core breakup

The breakup of the surface waves occurs when the surface waves grow to a critical size, given by the critical condition for droplet breakup of $We = \rho_g U^2 d_s/\sigma \approx 8.8$. The measured surface ligament sizes are compared to the theory in Figure B25. The measurements are found to be higher than the prediction. This is due to viscous effects, as the surface waves are sufficiently

small at this scale that viscosity plays a role in their breakup, despite the fluid being relatively inviscid.

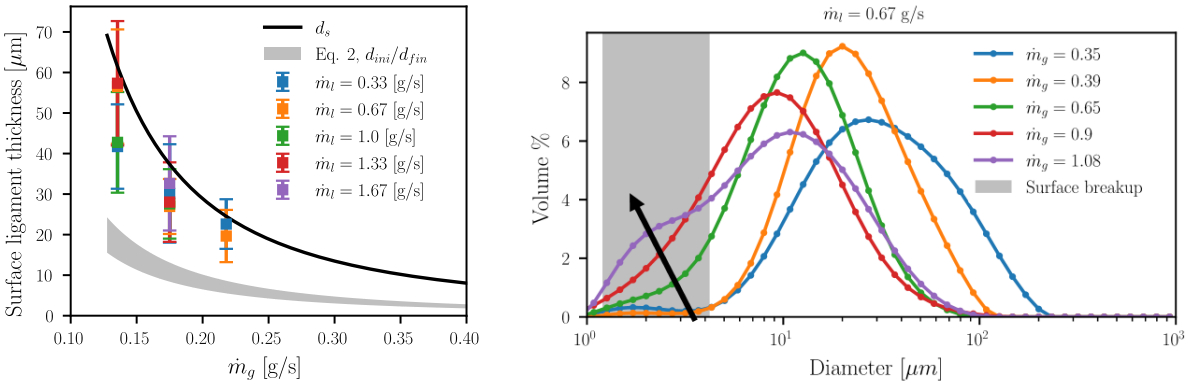

Figure B25: Comparison of theory of surface ligament thickness to measurements, and the effect of the surface breakup on the PSD.

The surface waves break at a characteristically small size. At low gas flow conditions, there is not enough surface breakup to dominate the volume distribution of the spray sizes. However, at higher flow rates, an additional mode in the PSD becomes apparent as the surface breakup begins to become important.

Understanding the balance between these three modes of breakup is crucial to understanding the proper operation of the spray. If there are too many large droplets due to intermittent core breakup, then the spray quality will be poor as too many large droplets will be produced. To counter this, the gas flow rate can be increased so that the core breaks up fully; however, at the extreme, too high of a gas flow rate also decreases the spray efficiency due to the over-production of fine droplets that do not settle in the drying air flow.

B.3. Elevated Temperatures

In typical spray-drying with two-fluid nozzles, the atomizing gas is not heated, and instead a secondary heated air flow is used to dry the resulting spray. Since the primary atomization occurs entirely before the atomizing air-stream mixes with the heated drying air-flow, there will be no effect of the heating drying air on the primary atomization. This is illustrated in Fig. B26.

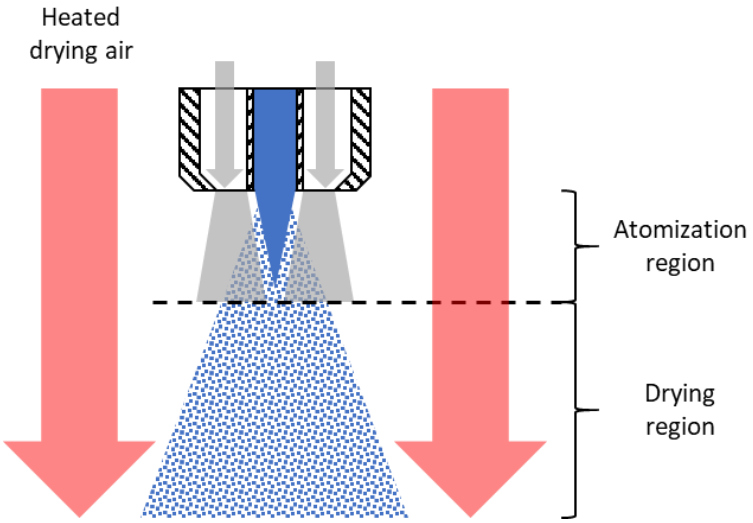

Figure B26: Illustration of the drying and atomizing air flow interaction with the primary atomization of the liquid jet.

While it would be possible to heat the atomizing air, the atomization time for two-fluid nozzles is so short that no significant heating of the liquid jet occurs. Using worst-case estimates for the heat transfer coefficient between the air and the liquid jet and the liquid jet diameter and atomization time, an atomizing air at 80°C above the liquid temperature would result in a heating of approximately 0.3°C of the liquid, which is not enough to significantly affect the evaporation rate or properties of the liquid. Furthermore, heating the atomizing air for a typical two-fluid nozzle is relatively wasteful, as the expansion of the air jet out of the nozzle results in a significant temperature drop in the air flow, substantially increasing the heating requirements to achieve the desired outlet air temperature. The main effect of doing so would be to allow for higher gas-flow speeds through the nozzle; however, this would be at the expense of a lower atomizing air density, which would partially negate any gain in performance from increasing the air speed. The effect of the heating on the air speed and density out of the nozzle is shown in Fig. B27. The heated air would likely have a greater effect over time on the nozzle body temperature, which would in turn heat the liquid and change its properties. However, it would be far more effective to simply heat the liquid directly to alter its properties; namely, lowering its viscosity.

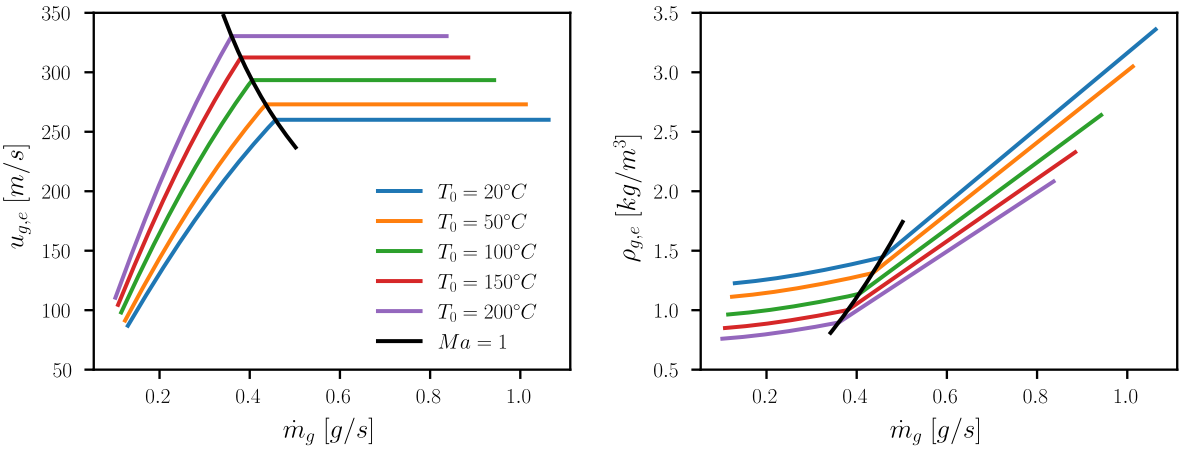

Figure B27: Effect of heating on the atomizing air speed and density.

Since the heated air flows are not expected to have a significant effect on the primary atomization of two-fluid nozzles, we have decided not to pursue this aspect of the investigation. However, for higher viscosity and polymeric fluids, the ligaments persist far downstream of the primary atomization region. In these cases, the effects of the heated airflow on the ligament breakup dynamics will be more important.

References

[1] Benchabane, A., and Bekkour, K., 2008, "Rheological Properties of Carboxymethyl Cellulose (CMC) Solutions," Colloid Polym. Sci., **286**(10), pp. 1173–1180.

[2] Chigier, N., and Farago, Z., 1992, "MORPHOLOGICAL CLASSIFICATION OF DISINTEGRATION OF ROUND LIQUID JETS IN A COAXIAL AIR STREAM," At. Sprays, **2**(2), pp. 137–153.

[3] Zhao, H., Liu, H. F., Xu, J. L., Li, W. F., and Cheng, W., 2012, "Breakup and Atomization of a Round Coal Water Slurry Jet by an Annular Air Jet," Chem. Eng. Sci., **78**, pp. 63–74.

[4] Varga, C. M., Lasheras, J. C., and Hopfinger, E. J., 2003, "Initial Breakup of a Small-Diameter Liquid Jet by a High-Speed Gas Stream," J. Fluid Mech., **497**(497), pp. 405–434.

[5] Aliseda, A., Hopfinger, E. J., Lasheras, J. C., Kremer, D. M., Berchielli, A., and Connolly, E. K., 2008, "Atomization of Viscous and Non-Newtonian Liquids by a Coaxial, High-Speed Gas Jet. Experiments and Droplet Size Modeling," Int. J. Multiph. Flow, **34**(2), pp. 161–175.

[6] Joseph, D. D., Belanger, J., and Beavers, G. S., 1999, "Breakup of a Liquid Drop Suddenly Exposed to a High-Speed Airstream," Int. J. Multiph. Flow, **25**, pp. 1263–1303.

[7] Joseph, D. D., Beavers, G. S., and Funada, T., 2002, "Rayleigh-Taylor Instability of Viscoelastic Drops at High Weber Numbers," J. Fluid Mech., **453**, pp. 109–132.

[8] Jackiw, I. M., and Ashgriz, N., 2021, "On Aerodynamic Droplet Breakup," J. Fluid Mech., **913**(A33).

[9] Zhao, H., Liu, H.-F., Li, W.-F., and Xu, J.-L., 2010, "Morphological Classification of Low Viscosity Drop Bag Breakup in a Continuous Air Jet Stream," Phys. Fluids, **22**(114103).

[10] Wang, Y., Dandekar, R., Bustos, N., Poulain, S., and Bourouiba, L., 2018, "Universal Rim Thickness in Unsteady Sheet Fragmentation," Phys. Rev. Lett., **120**(20), p. 204503.

[11] Guildenbecher, D. R., Gao, J., Chen, J., and Sojka, P. E., 2017, "Characterization of Drop Aerodynamic Fragmentation in the Bag and Sheet-Thinning Regimes by Crossed-Beam, Two-View, Digital in-Line Holography," Int. J. Multiph. Flow, **94**, pp. 107–122.